

Single file dynamics of tethered random walkers

S. B. Yuste¹, A. Baumgaertner², and E. Abad³

*¹Departamento de Física and Instituto de
Computación Científica Avanzada (ICCAEX)
Universidad de Extremadura,
E-06071 Badajoz, Spain*

*²Faculty of Physics, University of Duisburg-Essen,
47048 Duisburg, Germany*

*³Departamento de Física Aplicada and Instituto
de Computación Científica Avanzada (ICCAEX)
Centro Universitario de Mérida
Universidad de Extremadura,
E-06800 Mérida, Spain*

(Dated: February 26, 2025)

Abstract

We consider the single-file dynamics of N identical random walkers moving with diffusivity D in one dimension (walkers bounce off each other when attempting to overtake). Additionally, we require that the separation between neighboring walkers cannot exceed a threshold value Δ and therefore call them “tethered walkers” (they behave as if bounded by strings which tighten fully when reaching the maximum length Δ). For finite Δ , we study the diffusional relaxation to the equilibrium state and characterize the latter [the long-time relaxation is exponential with a characteristic time that scales as $(N\Delta)^2/D$]. In particular, our approximate approach for the N -particle probability distribution yields the one-particle distribution function of the central and edge particles [the first two positional moments are given as power expansions in $\Delta/\sqrt{4Dt}$]. For $N = 2$, we find an exact solution (both in the continuum case and on-lattice) and use it to test our approximations for one-particle distributions, positional moments, and correlations. For finite Δ and arbitrary N , edge particles move with an effective long-time diffusivity D/N , in sharp contrast with the $1/\ln(N)$ -behavior observed when $\Delta = \infty$. Finally, we compute the probability distribution of the equilibrium system length and the associated entropy. We find that the force required to change this length by a given amount is linear in this quantity, the (entropic) spring constant being $6k_B T/(N\Delta^2)$. In this respect, the system behaves like an ideal polymer. Our main analytical results are confirmed by Monte Carlo simulations.

PACS numbers: 05.40.Fb, 02.50.-r

I. INTRODUCTION

Diffusive transport in confined geometries continues to be a hot topic in many different fields nowadays, notably in biology. E.g., narrow channels are characterized by a width of the order of only a few particle diameters, and hence the simple paradigm of non-interacting diffusive particles clearly does not apply in this case, as excluded-volume effects and the influence of the confinement on other distance-dependent interactions must be taken into account.

Effectively one-dimensional natural and human-made systems in which diffusing particles are prevented from overtaking one another are abundant [1, 2]. This so-called single-file diffusion (SFD) results in the preservation of the initial particle ordering; an immediate

consequence is that diffusive mixing is strongly hindered, implying that a strong memory of the initial condition persists at long times. Another important consequence is that transport properties become strongly dependent on particle density, as the mean free path is greatly influenced by changes in this quantity. As pointed out by Bénichou *et al.* [2], these strong density effects are able to bring about drastic changes not only in transport coefficients, but also in the time dependence of key statistical quantities.

Unfortunately, we cannot account here for all the important theoretical and experimental contributions to the problem of SFD. We therefore restrict ourselves to a non-exhaustive list of a few of them. From an experimental point of view, SFD is relevant notably for transport in porous media [3, 4], hard rod systems [5, 6], traffic jams [7], protein diffusion in DNA [8, 9], the dynamics of trailing ants [10], sliding of ribosomes in messenger RNA [11], polymer translocation [12, 13], diffusion in zeolites [14–17], nanotubes [18], and confined colloidal systems [19–21]. Among the theoretical aspects are the calculation of propagators [21–26], the effect of different types of bias (due to autonomous motion or to external forces) [27], density profiles [28], large deviation functions [29–32], a broad class of correlation functions [33, 34], and first-passage properties [35, 36]. For more details see, e.g., Ryabov’s PhD thesis [1], the recent review by Bénichou *et al.* [2] and references therein.

The problem of diffusing particles subject to hard-core interactions in one dimension was considered by Harris in a pioneering work [37]. This author found that the positional probability density function (pdf) of a tracer particle remains Gaussian, but its mean square displacement (MSD) displays subdiffusive behavior of the form $\langle x^2 \rangle \propto t^{1/2}$, as opposed to the normal diffusive behavior observed for non-interacting particles. Kollmann demonstrates in Ref. [21] that this behavior occurs for any type of interaction between particles, provided that mutual passage is excluded. The independence from the details of the interaction potential between particles is exploited by Lizana *et al.* [38] to develop a harmonization method. In this method, the true potential (which includes a hard-core part) between the particles is replaced by a harmonic potential. This substitution facilitates the analytical treatment of SFD systems.

Beyond the observed onset of anomalous diffusion [39, 40], we have already mentioned above that another hallmark of single file systems is their non-Markovian character due to correlations between particles, which results in strong memory effects [41, 42]. In this context, it is worth mentioning the importance of finite-size effects. As already mentioned,

for the infinite system considered in Ref. [37] the behavior of the tracer particle in the long-time asymptotic regime is subdiffusive; in contrast, for a finite system, subdiffusion is only transient, and a crossover to normal diffusion takes place as $t \rightarrow \infty$. While the thermodynamic limit is very popular in the existing literature on both continuum and on-lattice SFD, the case of a finite particle number bears special relevance for biological systems, as narrow channels typically harbor simultaneously a very limited number of particles [43–45].

In the present work, we address the problem of SFD in the case where the interacting potential is non-analytic and the number of particles N is finite. Before proceeding to outline the contents of each section, let us briefly discuss a few works that are of special relevance for our purposes. The intimate connection between reflected Brownian motion [46–49] and single file transport has been exploited by a number of authors to study the properties of many systems of interest. Rödenbeck, Kärger and Hahn devised a method based on the reflection principle to calculate exact propagators for a general class of single-file systems [22]. They took advantage of the fact that the derivative normal to the plane defined by equating the coordinates of any two particles must vanish (zero-flux condition), and that the corresponding solution can be constructed by the method of images. At about the same time, Aslangul [23] used a factorization ansatz based on a product of Gaussian propagators and step functions to obtain an exact solution for the N -particle propagator that satisfies the zero-flux condition in the aforementioned planes. From the propagator, Aslangul was able to compute the drift and diffusion properties arising from the many-body interactions. In a subsequent work [24], he compared the off-lattice solution with the lattice solution and found that the signature of the discrete spatial support persists for a long time in the solution via long-lived subdominant contributions.

Here, we go one step further and investigate the effect of imposing a second constraint on diffusing particles subject to hard-core interactions, namely, that the separation distance between each particle and either of its nearest-neighbors never exceed a fixed value Δ . We will hereafter often refer to such particles as “tethered walkers”. In order to visualize our setting, the walkers can be thought of as being linked to one another by strings which tighten progressively as they move away from each other but have otherwise no influence on the motion as long as the allowed maximum separation distance Δ (length of the string) is not exceeded. In this case, the string exerts an infinite instantaneous attractive force which

avoids further growth of the separation distance; in other words, each walker carries with her a symmetric infinite potential well (a hard-wall potential) of width Δ that limits the motion of both nearest neighbors. In this sense, loosely speaking our model can be viewed as a “string-bead” model rather than a spring-bead one.

Let us briefly anticipate how our “string-bead” system behaves. Unless otherwise specified, we will consider a fully packed initial condition in which all the walkers start at the origin. As the walkers diffuse, they first separate from each other without crossing, but then the action of the Δ constraint starts to become noticeable. This trade-off between the single-file constraint and the Δ -constraint results in relaxation towards an equilibrium state which is attained after a time of the order $(N\Delta)^2/D$, where D is the coefficient of diffusion of isolated, freely moving particles. In what follows, we aim to study particle diffusion as a mechanism of relaxation to the equilibrium steady state. For large N , we will characterize the latter from the point of view of statistical thermodynamics and also assess to what extent this system resembles a linear chain in a viscous medium, i.e. a polymer chain in a solvent [50, 51].

In the above context, we stress the difficulty of dealing with the nonanalytic interaction potential prescribed by the Δ constraint, as opposed to other types of interactions, such as the harmonic potential that connects neighboring beads in the celebrated Rouse model (see e.g. Ref. [52]). There is a significant difference between the latter and the interaction potential associated with our tethered walkers. From the point of view of the calculations, an exact solution in the latter case only seems possible for a two-particle system ($N = 2$).

In the absence of the Δ -constraint, i.e., for $\Delta = \infty$, one expects significant differences between the behavior of the edge particles and those in the bulk even in the long time regime. Aslangul’s analysis for this case [23] shows that at long times the central particle has an effective diffusivity equal to D/N , whereas the effective diffusivity of the edge particle decreases only as $1/\ln(N)$. In contrast, we find that this difference in behavior disappears as soon as Δ becomes finite, since then all the particles diffuse with the same effective diffusivity D/N at sufficiently long times. We then complement our study of diffusional relaxation with the calculation of the probability distribution of the equilibrium system length and the associated entropy. The force required to change the length by a given amount is linear in this quantity, the (entropic) spring constant being equal to $6k_B T/(N\Delta^2)$. In this respect, the system behaves like a polymer modeled by an ideal chain. Finally, we confirm our main

results with Monte Carlo simulations.

The remainder of this paper is organized as follows. Sec. II describes the N -walker system in detail and the approximate factorization ansatz used for the analytical treatment for the positional pdf and other quantities of interest. Sec. III focuses on the approximate solution obtained in this way for the specific case $N = 2$. Next, in Sec. IV, an exact solution for $N = 2$ is given, thoroughly discussed, and compared with the approximate one obtained in the previous section. Sec. V deals with the $N = 3$ case. Sec. VI is devoted to the approximate solution for arbitrary N and to the study of its relaxation to the equilibrium state. The latter is comprehensively studied in Sec. VII. The main conclusions and perspectives are summarized in Sec. VIII. The appendices A, B, and C are devoted to different aspects of the $N = 2$ case, namely, the approximate calculation of higher odd-order moments, the extension of the exact solution when both particles are initially separated by a finite distance, and the on-lattice solution.

II. N -PARTICLE PDF

We consider a collection of N point walkers with a common diffusivity D on the real line, their respective positions being x_1, x_2, \dots, x_N . Denoting the initial coordinate of the j -th walker by x_j^0 , we henceforth assume $x_1^0 \leq x_2^0, \dots, x_{N-1}^0 \leq x_N^0$. The walkers perform SFD, implying that they bounce off each other when they attempt to overtake. Thus, the initial ordering is preserved, i.e., $x_1 \leq x_2, \dots, x_{N-1} \leq x_N$ at all times, and the system is in this respect similar to the one studied in Ref. [23]. In this reference, the study is restricted to the fully packed initial condition $x_1^{(0)} = x_2^0 = \dots = x_N^0 = 0$. Here, we will also focus mainly on this case, but our formulation holds for a general initial condition. As a novelty, we now include an additional constraint, which consists in preventing the walkers from travelling too far from each other. Specifically, the j -th walker is not allowed to separate farther than a distance Δ from either neighbor, i.e., one must always have $|x_j - x_{j\pm 1}| \leq \Delta$. As soon as any walker tries to violate this condition, the Δ -constraint acts as a tether which impedes the walker to move further away from its neighbor. As we shall see, the SFD of such “tethered” walkers is drastically different from walkers subject to the non-crossing restriction only.

Inspired by the analytical approach of Ref. [23], in what follows we assume that the N -

particle positional pdf of the tethered-walker system can be approximated by the product

$$p_x(x_1, x_2, \dots, x_N, t; \Delta) = B \prod_{i=1}^N G(x_i, t|x_i^0) \prod_{i=1}^{N-1} R(x_{i+1} - x_i, \Delta), \quad (1)$$

where B is a normalization constant, $G(x, t|x^0)$ is the free-particle Green function (Gaussian distribution)

$$G(x, t|x^0) = \frac{e^{-(x-x^0)^2/4Dt}}{\sqrt{4\pi Dt}}, \quad (2)$$

and $R(x, \Delta)$ denotes the rectangular function of width Δ defined as follows:

$$R(x, \Delta) = \begin{cases} 1 & \text{for } 0 < x < \Delta, \\ 0 & \text{elsewhere.} \end{cases} \quad (3)$$

Equation (2) accounts for the normal diffusion of particles with diffusion coefficient D when they move freely. The rectangular function ensures that particles do not cross each other and that nearest neighbors are separated by no more than a distance Δ .

We will henceforth focus on the case of a packed initial state $x_j^0 \equiv 0 \forall j$, which is the case addressed in Ref. [23]. The calculations become significantly less cumbersome if one switches to the dimensionless variables $u = x/\sqrt{4Dt}$ and $\delta \equiv \delta(t) = \Delta/(4Dt)^{1/2}$, which respectively denote the scaled coordinate and reach of interaction. The coordinate scaling must, however, ensure probability conservation, i.e.,

$$p_x(x_1, \dots, x_N, t; \Delta) dx_1 \dots dx_N = p(u_1, \dots, u_N; \delta) du_1 \dots du_N, \quad (4)$$

which implies

$$p(u_1, u_2, \dots, u_N; \delta) = (4Dt)^{N/2} p_x(x_1, \dots, x_N; \Delta = \delta \sqrt{4Dt}), \quad (5)$$

with $x_i = u_i \sqrt{4Dt}$, or, equivalently,

$$p(u_1, u_2, \dots, u_N; \delta) = A \prod_{i=1}^N e^{-u_i^2} \prod_{i=1}^{N-1} R(u_{i+1} - u_i, \delta), \quad (6)$$

where $A = B/\pi^{N/2}$ is the corresponding normalization constant.

At the single-particle level, one can define the reduced one-particle pdf $p_n^{(1)}(x_n, t, \Delta)$ via a multiple integral:

$$\begin{aligned} p_n^{(1)}(x_n, t, \Delta) &= \int_{-\infty}^{\infty} \dots \int_{-\infty}^{\infty} dx_1 \dots dx_{n-1} dx_{n+1} \dots dx_N p(x_1, x_2, \dots, x_N, t; \Delta) \\ &= (4Dt)^{1/2} \int_{-\infty}^{\infty} \dots \int_{-\infty}^{\infty} du_1 \dots du_{n-1} du_{n+1} \dots du_N p(u_1, u_2, \dots, u_N; \delta) \\ &= (4Dt)^{1/2} p_n^{(1)}(u_n, \delta), \end{aligned} \quad (7)$$

where, for brevity, we have dropped the subindex “ x ” in $p_x(x_1, x_2, \dots, x_N, t; \Delta)$. In what follows, we use this simplified notation, and we will also omit the explicit reference to Δ both in p_x and in the reduced probabilities $p_n^{(1)}$ unless stated otherwise. The one-particle moments defined in terms of original and scaled coordinates are related to one another as follows:

$$\langle x_n^m \rangle(t) = \int_{-\infty}^{\infty} dx_n x_n^m p_n^{(1)}(x_1, t) = (4Dt)^{m/2} \int_{-\infty}^{\infty} du_n u_n^m p_n^{(1)}(u_1, \delta) = (4Dt)^{m/2} \langle u_n^m \rangle(\delta) \quad (8)$$

In particular, the variance $\text{Var}(x_n) \equiv \langle x_n^2 \rangle - \langle x_n \rangle^2$ of the n -th walker position (also termed “centered MSD” hereafter) can now be expressed in terms of rescaled moments:

$$\text{Var}(x_n) = \text{Var}(u_n) 4Dt = 4D_{\text{eff}}(t) t, \quad (9)$$

where

$$D_{\text{eff}}(t) = D \text{Var}(u_n) \quad (10)$$

We will see later that $\text{Var}(u_n) \equiv \langle u_n^2 \rangle - \langle u_n \rangle^2$ (and therefore also D_{eff}) depends on time, indicating the existence of anomalous diffusion. In fact, the term “transient anomalous diffusion” is pertinent here, since at very long times the diffusion becomes normal (albeit with an N -dependent effective diffusivity). We will discuss this behavior in more detail at the appropriate stage.

III. $N = 2$ CASE: APPROXIMATE RESULTS

The two-particle case is amenable to exact solution and therefore worth a separate treatment. In Ref. [24], an exact solution (both on- and off-lattice) was given for the case $\Delta = \infty$, i.e., when the separation between the walkers can become arbitrarily large. In what follows, we will address the case with finite Δ . We will mainly focus on the continuum limit (off-lattice) solution, but also give some on-lattice results. In this section, we will obtain approximate results for the continuum case based on the factorization ansatz (1), which will then be compared with the exact solution obtained in Sec. IV.

A. Positional pdf

According to Eq. (6) the scaled two-particle pdf is

$$p(u_1, u_2) \equiv p(u_1, u_2; \delta) = A e^{-u_1^2} e^{-u_2^2} R(u_2 - u_1, \delta). \quad (11)$$

The reduced one-particle pdfs are defined by Eq. (7), which in the present case yields

$$p_1^{(1)}(u_1, \delta) = A e^{-u_1^2} \int_{u_1}^{u_1+\delta} du_2 e^{-u_2^2}, \quad (12)$$

$$p_2^{(1)}(u_2, \delta) = A e^{-u_2^2} \int_{u_2-\delta}^{u_2} du_1 e^{-u_1^2} \quad (13)$$

(recall that, in our notation, the subscripts 1 and 2 refer to the left and right particle, respectively). The above integrals (as well as the normalization constant A) can be expressed in terms of the error function $\text{Erf}(z) = (2/\sqrt{\pi}) \int_0^z du e^{-u^2}$. One finds

$$p_1^{(1)}(u_1, \delta) = \frac{\text{Erf}(u_1 + \delta) - \text{Erf}(u_1)}{\sqrt{\pi} \text{Erf}(\delta/\sqrt{2})} e^{-u_1^2} \quad (14)$$

and $p_2^{(1)}(u_2, \delta) = -p_1^{(1)}(u_2, -\delta)$. We have used the result [53]

$$\int_{-\infty}^{\infty} du e^{-u^2} \text{Erf}(u + C) = \sqrt{\pi} \text{Erf}(C/\sqrt{2}). \quad (15)$$

In terms of the original coordinate, the above expressions respectively give (in full notation)

$$p_1^{(1)}(x_1, t, \Delta) = \frac{1}{\text{Erf}(\Delta/\sqrt{8Dt})} \left[\text{Erf}\left(\frac{x_1 + \Delta}{\sqrt{4Dt}}\right) - \text{Erf}\left(\frac{x_1}{\sqrt{4Dt}}\right) \right] \frac{e^{-x_1^2/4Dt}}{\sqrt{4\pi Dt}} \quad (16)$$

for the left particle and

$$p_2^{(1)}(x_2, t, \Delta) = -p_1^{(1)}(x_2, t, -\Delta) \quad (17)$$

for the right particle.

In Fig. 1 we compare simulation results for the reduced probability $p_1^{(1)}(x_1, t)$ with the approximate theoretical expression (16) and with Aslangul's result for $\Delta = \infty$. The exact analytical solution given by Eq. (54) is included in the figure as well (see Sec. IV). The agreement between the approximation and the simulations/exact result is good as long as the diffusion approximation holds, which requires that Δ remain large in comparison with the typical jump length used in the simulations. In the simulations shown in Fig. 1, the average jump length and the average waiting time between consecutive jumps are used as the units of length and time, respectively. Both jump lengths and waiting times are drawn from exponential distributions.

B. First-order moment

Using the result

$$\int_{-\infty}^{\infty} du u e^{-u^2} \text{Erf}(u + C) = \frac{1}{\sqrt{2}} e^{-C^2/2}, \quad (18)$$

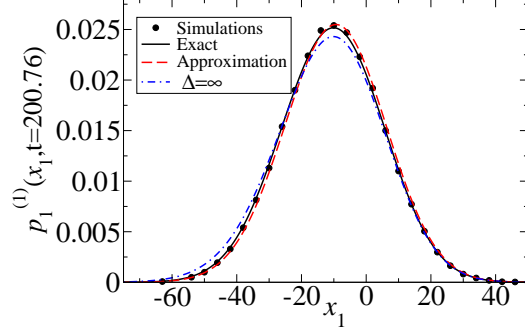


FIG. 1. Simulated pdf $p_1^{(1)}(x_1, t)$ for $N = 2$ (circles). We have taken $D = 1$, $t = 200.76$, and $\Delta = 50$, which gives $\delta = 1.7644$. The solid line represents the exact solution (54). The dashed lined is the approximate theoretical expression (16). Finally, the dashed-dotted line corresponds to the case in which the impenetrable particles can move without any further limitation (i.e., $\Delta = \infty$).

one finds upon use of Eq. (14) the result

$$\langle u_2 \rangle = -\langle u_1 \rangle = \frac{1 - e^{-\delta^2/2}}{\text{Erf}(\delta/\sqrt{2})} \sqrt{\frac{1}{2\pi}} \quad (19)$$

In terms of the rescaled variable, one thus has

$$\langle x_2 \rangle = -\langle x_1 \rangle = \frac{1 - e^{-\Delta^2/8Dt}}{\text{Erf}(\Delta/\sqrt{8Dt})} \sqrt{\frac{2}{\pi}Dt}. \quad (20)$$

For large δ , i.e., for $\Delta \rightarrow \infty$ or $t \rightarrow 0$ (early time regime¹) one recovers the result given by Eq. (6) in Ref. [23], namely, $\langle x_2 \rangle = -\langle x_1 \rangle = \sqrt{\frac{2}{\pi}Dt}$. For the $\Delta = \infty$ case addressed in that reference, this expression is valid for arbitrarily large times, and the particle drift grows without bound in this limit. Returning to the case of finite Δ , if we incorporate the next correction term in the expansion of the right-hand side (rhs) of Eq. (20), we are then left with the expression

$$\langle x_2 \rangle \approx \sqrt{\frac{2}{\pi}Dt} (1 - e^{-\Delta^2/8Dt}), \quad (21)$$

i.e., our approximation shows that the influence of a finite Δ -value becomes noticeable when it becomes comparable to \sqrt{Dt} . In the opposite limit of small δ or long times t , one can use

¹ Note that the limit $t \rightarrow 0$ must be understood in the usual sense in the context of diffusion, i.e. on the one hand the times t are still long enough for the walker to have performed a large number of jumps $N_{\text{jump}} \gg 1$, but on the other hand short enough to ensure that Dt remains small for a given value of D .

the asymptotic expansion

$$\frac{1 - e^{-z^2}}{\text{Erf}(z)} = \frac{\pi z}{2} - \frac{\sqrt{\pi} z^3}{12} + \mathcal{O}(z^5), \quad z \rightarrow 0 \quad (22)$$

in Eq. (20) to obtain

$$\frac{\langle x_2 \rangle}{\Delta} = \frac{1}{4} - \frac{\Delta^2}{192Dt} + \mathcal{O}\left(\frac{\Delta^2}{Dt}\right)^2, \quad t \rightarrow \infty. \quad (23)$$

Thus, for finite Δ , Eq. (20) yields a finite first-order moment as $t \rightarrow \infty$, i.e., $\langle x_2 \rangle = -\langle x_1 \rangle \rightarrow \Delta/4$ (or, equivalently, $\langle u_2 \rangle = -\langle u_1 \rangle = \delta/4$ as $\delta \rightarrow 0$). According to Eq. (23), the relaxation to the limiting value of $\langle x_2 \rangle$ is eventually controlled by the inverse power-law $(Dt)^{-1}$.

Finally, we note that it is possible to extend the above approximate analysis for the first-order moment to arbitrary odd-order moments (see Appendix A).

C. Second-order moment

The evaluation of the scaled second-order moment

$$\langle u^2 \rangle \equiv \langle u_2^2 \rangle = \langle u_1^2 \rangle = \int_{-\infty}^{\infty} du u^2 p_1^{(1)}(u, \delta) \quad (24)$$

is complicated by the fact that an analytic expression for the integral

$$\int_{-\infty}^{\infty} du u^2 e^{-u^2} \text{Erf}(u + \delta) \quad (25)$$

must be found. We have not succeeded in doing so and thus we are led to perform series expansions for small and large values of δ .

1. Small- δ expansion

To evaluate the rhs of Eq. (24) for small values of δ (large values of t), one could directly expand $\text{Erf}(u + \delta)$ in powers of δ and carry out the corresponding integrals. However, we will follow a less direct route which will later be conveniently extended to the case $N > 2$. From the definition of the error function, one has

$$p_1^{(1)}(u_1, \delta) = \frac{2 e^{-u_1^2}}{\pi \text{Erf}(\delta/\sqrt{2})} \int_{u_1}^{u_1+\delta} e^{-u_2^2} du_2. \quad (26)$$

To begin with, we expand $e^{-u_2^2}$ around u_1 as follows (we will keep three terms in the expansions; finding higher order terms is immediate):

$$e^{-u_2^2}/e^{-u_1^2} = 1 - 2u_1(u_2 - u_1) - (1 - 2u_1^2)(u_2 - u_1)^2 + \mathcal{O}((u_2 - u_1)^3). \quad (27)$$

Consequently,

$$e^{u_1^2} \int_{u_1}^{u_1+\delta} du_2 e^{-u_2^2} = \delta - u_1\delta^2 - \frac{1}{3}(1 - 2u_1^2)\delta^3 + \mathcal{O}(\delta^4). \quad (28)$$

Therefore, the reduced one-particle pdf can be written as follows:

$$p_1^{(1)}(u_1, \delta) = \frac{2e^{-2u_1^2}}{\pi \text{Erf}(\delta/\sqrt{2})} \left[\delta - u_1\delta^2 - \frac{1}{3}(1 - 2u_1^2)\delta^3 + \mathcal{O}(\delta^4) \right] \quad (29)$$

Note that the expression also follows directly by using the pertinent expansion in Eq. (14).

The second-order moment is obtained by inserting Eq. (29) into Eq. (24), carrying out the integrations, and finally expanding the result in powers of δ . This gives

$$\langle u_1^2 \rangle = \langle u_2^2 \rangle = \frac{1}{4} + \frac{\delta^2}{12} - \frac{\delta^4}{90} + \mathcal{O}(\delta^6). \quad (30)$$

Note that $\langle u_{1,2}^2 \rangle = 1/4 = 1/(2N)$ as $\delta \rightarrow 0$, i.e., as $t \rightarrow \infty$ for a prescribed Δ . Thus, $\langle x_{1,2}^2 \rangle = Dt$, that is, the effective diffusion coefficient of either particle tends to $D/2$ (recall that $\langle x^2 \rangle = 2Dt$ for a single particle). This result is consistent with the Rouse model for polymers, where the diffusion coefficient of a chain with N beads is D/N given the diffusion coefficient D of a single bead [54]. The moments in terms of the original coordinates are obtained by undoing the scaling in Eq. (30):

$$\langle x_1^2 \rangle = \langle x_2^2 \rangle = Dt + \frac{\Delta^2}{12} - \frac{\Delta^4}{360Dt} + \mathcal{O}\left(\frac{\Delta^6}{D^2t^2}\right). \quad (31)$$

2. Large- δ expansion

The small- δ expansion of $\langle u^2 \rangle$ can be complemented with the analysis of the opposite limit (large δ). In what follows, we will use the asymptotic expansion of the error function to obtain approximations for the integral leading to $\langle u^2 \rangle$. One has [53]

$$\text{Erf}(z) = 1 - \frac{e^{-z^2}}{\sqrt{\pi}z} \left[\sum_{k=0}^{N-1} (-1)^k \frac{(2k-1)!!}{(2z^2)^k} + \mathcal{O}(|z|^{2-2N}) \right], \quad z \rightarrow \infty. \quad (32)$$

Setting $z = u + \delta$ and using the above expansion, one finds

$$\text{Erf}(u + \delta) = 1 - \frac{e^{-(u+\delta)^2}}{\sqrt{\pi}\delta} \left[1 + \frac{u}{\delta} + \frac{\frac{1}{2} - u}{\delta^2} + \mathcal{O}(\delta^{-3}) \right], \quad \delta \rightarrow \infty \quad (33)$$

The above expansion can be used as a starting point to obtain approximations for

$$\langle u^2 \rangle = \frac{1}{\sqrt{\pi} \text{Erf}(\delta/\sqrt{2})} \int_{-\infty}^{\infty} du u^2 e^{-u^2} \text{Erf}(u + \delta). \quad (34)$$

E.g., retaining terms up to order δ^{-2} in the brackets in the rhs of Eq. (33), one finds

$$\langle u^2 \rangle \approx \frac{1}{2\text{Erf}(\delta/\sqrt{2})} \left[1 - \frac{e^{-\delta^2/2}(1 + 14\delta^2 + 7\delta^4)}{8\sqrt{2\pi}\delta^3} \right] \quad (35)$$

(expressions for higher even-order moments can also be obtained by using the expansion (33) in the corresponding integrals). From Eqs. (35), (19) and (10) one finds that the (dimensionless) effective diffusion coefficient is

$$\frac{D_{\text{eff}}}{D} = \frac{1}{2} \left(1 - \frac{1}{\pi} \right) - \frac{7}{16\sqrt{2\pi}} \delta e^{-\delta^2/2} + \dots \quad (36)$$

In terms of unscaled coordinates,

$$\langle x^2 \rangle = 2Dt - \frac{7}{8\sqrt{2\pi}} \Delta \sqrt{Dt} e^{-\Delta^2/(8Dt)} + \dots \quad (37)$$

Together with our result (21) for the first moment, Eq. (37) implies

$$\text{Var}(x) = 2 \left(1 - \frac{1}{\pi} \right) Dt - \frac{7}{8\sqrt{2\pi}} \Delta \sqrt{Dt} e^{-\Delta^2/(8Dt)} + \dots \quad (38)$$

For times short enough to ensure that the Δ -constraint does not play a noticeable role, one recovers Aslangul's result $\text{Var}(x) \sim 2(1 - \pi^{-1})Dt$ in the $\Delta = \infty$ case; i.e., the diffusion is normal, but the particle diffusivity is decreased with respect to the case of free particles by the single-file constraint. Physically, this makes sense, but we recall that our solution is only approximate (based on the factorization ansatz), and the validity of this expression for the long time limit must therefore be assessed by simulations and by the exact solution, which is available in the present $N = 2$ case.

D. Correlator

The two-particle correlation function $C(t) \equiv \langle x_1 x_2 \rangle - \langle x_1 \rangle \langle x_2 \rangle$ can be written in terms of the variable u as follows:

$$C(t) = 4Dt c(t) \quad (39)$$

with

$$c(t) = c(\delta) = \langle u_1 u_2 \rangle - \langle u_1 \rangle \langle u_2 \rangle. \quad (40)$$

After elementary calculations, one finds

$$\langle u_1 u_2 \rangle = \int_{-\infty}^{\infty} du_1 du_2 u_1 u_2 p(u_1, u_2) = \frac{A}{4} \sqrt{\frac{\pi}{2}} \delta e^{-\delta^2/2}, \quad (41)$$

where the normalization factor is $A = (\sqrt{\pi} \operatorname{Erf}(\delta/\sqrt{2}))^{-1}$. Thus, using Eq. (41) and Eq. (19), one eventually arrives at the result

$$c(\delta) = \frac{(1 - e^{-\delta^2/2})^2}{2\pi \operatorname{Erf}^2(\delta/\sqrt{2})} + \frac{\delta e^{-\delta^2/2}}{4\sqrt{2} \operatorname{Erf}(\delta/\sqrt{2})}. \quad (42)$$

Even for large δ , one has non-zero correlations due to particle repulsion as a result of collisions at short times. At smaller δ (or sufficiently long times), both particles start to feel the additional effect of the Δ constraint, as a result of which the correlation increases.

One further has the limiting values $c(\delta \rightarrow 0) = 1/4$ and $c(\delta \rightarrow \infty) = 1/(2\pi)$. The latter is consistent with the expression $C(t) = 2Dt/\pi$ obtained in [23] for $\Delta = \infty$, which is valid for arbitrary t . As expected, the influence of the finite interaction range is negligible at short times, and the result for $\Delta = \infty$ is recovered.

IV. $N = 2$ CASE: EXACT SOLUTION

In the case $N = 2$, it is possible to obtain an exact solution by mapping the problem to a problem of diffusion of a single particle in the plane with tilted reflected boundaries. To illustrate how the method works, we will first deal with the well-known $\Delta = \infty$ case.

A. Case of infinite range ($\Delta = \infty$)

The evolution of both particles can be interpreted as a two-dimensional diffusion of a single particle with coordinates (x_1, x_2) , constrained to move within one of the half-planes bounded by the reflecting line $x_2 = x_1$. The initial condition when both particles start at the origin is of course $(x_1^0, x_2^0) \equiv (0, 0)$.

To determine the probability $p_{\infty}(x_1, x_2, t) \equiv p_x(x_1, x_2, t; \Delta = \infty)$ of the single diffusing particle being at position (x_1, x_2) at time t , we first calculate the probability $p_{\infty}^{\text{hor}}(x_1, x_2, t)$ for a single diffusing particle to be at position (x_1, x_2) at time t when the reflecting line is the horizontal axis ($x_2 = 0$). This probability is well-known. It can e.g. be obtained by regarding the line as a two-dimensional wedge with reflecting edges and spread angle π .

This allows one to exploit the solution for diffusion in a three-dimensional wedge given in the monograph by Carslaw and Jaeger (see Eq. (8) on p. 379 of Ref. [55]) by using the corresponding reduced pdf, which is obtained by integrating out the transversal degree of freedom x_3 . This gives

$$p_{\infty}^{\text{hor}}(x_1, x_2, t) = \frac{e^{-(x_1^2+x_2^2)/4Dt}}{2\pi Dt} \Theta(x_2). \quad (43)$$

An alternative way of obtaining the above solution relies upon the observation that the boundary condition only affects the vertical degree of freedom. Since the x_1 - and x_2 evolutions are uncoupled, the solution (43) can be obtained as the product of the free one-dimensional Gaussian $e^{-x_1^2/4Dt}/\sqrt{4\pi Dt}$ for the horizontal coordinate x_1 times the one-dimensional solution $\Theta(x_2) e^{-x_2^2/4Dt}/\sqrt{\pi Dt}$ corresponding to diffusion on the halfline $x_2 > 0$ with a reflecting endpoint at $x_2 = 0$.

The solution (43) satisfies the zero normal flux condition $\partial_{x_2} p(x_1, x_2, t)|_{x_2=0}=0$. In contrast, the solution that we seek must satisfy a similar boundary condition on the tilted reflecting line, i.e., $\mathbf{n}_{\perp} \cdot \nabla p(x_1, x_2, t)|_{x_2=x_1} = 0$, where $\mathbf{n}_{\perp} \equiv (1/\sqrt{2}, -1/\sqrt{2})$ denotes the unit vector perpendicular to the reflecting line. In order to obtain the desired solution, we must now rotate the solution (43) by 45 degrees about an axis perpendicular to (x_1, x_2) that goes through the origin. This rotation is performed via the unitary transformation $x_1 \rightarrow (x_2 + x_1)/\sqrt{2}$, $x_2 \rightarrow (x_2 - x_1)/\sqrt{2}$, which yields

$$p_{\infty}(x_1, x_2, t) = \frac{e^{-(x_1^2+x_2^2)/4Dt}}{2\pi Dt} \Theta(x_2 - x_1). \quad (44)$$

This is precisely the solution obtained by Aslangul with his product ansatz for the $N = 2$ case [23], from which we conclude that his procedure is *exact* in this case.

The exact computation of the corresponding integer order moments

$$\langle x_2^m \rangle \equiv \int_{-\infty}^{\infty} dx_1 \int_{-\infty}^{\infty} dx_2 x_2^m p_{\infty}(x_1, x_2, t) = (-1)^m \langle x_1^m \rangle \quad (45)$$

is now straightforward. We obtain

$$\langle x_2^m \rangle = \begin{cases} \pi^{-1/2} \Gamma(\frac{m+1}{2}) (4Dt)^{m/2}, & \text{for } m \text{ even,} \\ 2^{1/2} \pi^{-1} {}_2F_1(\frac{1}{2}, \frac{1-m}{2}, \frac{3}{2}, \frac{1}{2}) \Gamma(\frac{m}{2} + 1) (4Dt)^{m/2}, & \text{for } m \text{ odd,} \end{cases} \quad (46)$$

where ${}_2F_1(\cdot)$ stands for a confluent hypergeometric function. The expression for even m can be further simplified by means of Legendre's duplication formula $\Gamma(z)\Gamma(z + 1/2) =$

$2^{1-2z}\sqrt{\pi}\Gamma(2z)$. In terms of the variable u , we find

$$\langle u_2^m \rangle = \frac{\langle x_2^m \rangle}{(4Dt)^{m/2}} = \begin{cases} 2^{-m}m!/(m/2)!, & \text{for } m \text{ even,} \\ 2^{1/2}\pi^{-1}{}_2F_1(\frac{1}{2}, \frac{1-m}{2}, \frac{3}{2}, \frac{1}{2})\Gamma(\frac{m}{2}+1), & \text{for } m \text{ odd.} \end{cases} \quad (47)$$

These results confirm Aslangul's findings for the particular cases $m = 1$ and $m = 2$, namely, $\langle x_2 \rangle = (2Dt/\pi)^{1/2}$ and $\langle x_2^2 \rangle = 2Dt$.

B. Case of finite Δ

Once again, the dynamics can be viewed as two-dimensional diffusion of one particle confined by two parallel reflecting lines at $x_2 = x_1$ and $x_2 = x_1 + \Delta$ and starting at $(0, 0)$. Note that this is motion inside a tilted strip of thickness $\Delta/\sqrt{2}$. The probability $p(x_1, x_2, t)$ of finding the single diffusing particle at position (x_1, x_2) at time t on this tilted strip is obviously related to the probability $p^{\text{hor}}(x_1, x_2, t)$ for the horizontal strip limited by two parallel reflecting lines at $x_2 = 0$ and $x_2 = \Delta/\sqrt{2}$. The non-tilted solution $p^{\text{hor}}(x_1, x_2, t)$ can be straightforwardly obtained from the solution for the three-dimensional wedge given in Ref. [55] [cf. Eq. (18) on p. 374] for diffusion confined by two fully reflecting parallel *planes* oriented along the x_1 -axis. Integrating out the third coordinate x_3 in the solution yields:

$$p^{\text{hor}}(x_1, x_2, t) = \frac{\sqrt{2}}{\Delta} \left\{ 1 + 2 \sum_{n=1}^{\infty} e^{-2n^2\pi^2Dt/\Delta^2} \cos\left(\frac{n\pi\sqrt{2}}{\Delta}x_2\right) \right\} R(x_2, \frac{\Delta}{\sqrt{2}}) \times \frac{e^{-x_1^2/4Dt}}{\sqrt{4\pi Dt}}. \quad (48)$$

The rhs is again the product of two solutions, namely, a free Gaussian corresponding to the horizontal degree of freedom, and another solution corresponding to diffusion on a finite interval with reflecting endpoints at $x_2 = 0$ and $x_2 = \Delta/\sqrt{2}$. Using the method of images, Eq. (48) can be conveniently rewritten as follows [cf. Eq. (19) on p. 374 of Ref. [55]]:

$$p^{\text{hor}}(x_1, x_2, t) = \left\{ \sum_{n=-\infty}^{\infty} e^{(-n^2\Delta^2 + \sqrt{2}nx_2\Delta)/2Dt} \right\} R(x_2, \frac{\Delta}{\sqrt{2}}) \times \frac{e^{-(x_1^2+x_2^2)/4Dt}}{2\pi Dt}. \quad (49)$$

To find the exact solution of our problem, we now perform the anticlockwise rotation of p_{hor} by 45 degrees, implying that the resulting solution must fulfil the boundary conditions $\mathbf{n}_{\perp} \cdot \nabla p(x_1, x_2, t)|_{x_2=x_1} = 0$ and $\mathbf{n}_{\perp} \cdot \nabla p(x_1, x_2, t)|_{x_2=x_1+\Delta} = 0$. This yields

$$p(x_1, x_2, t) = \Upsilon(x_2 - x_1, \Delta, t) \Theta(\Delta - (x_2 - x_1)) p_{\infty}(x_1, x_2, t), \quad (50)$$

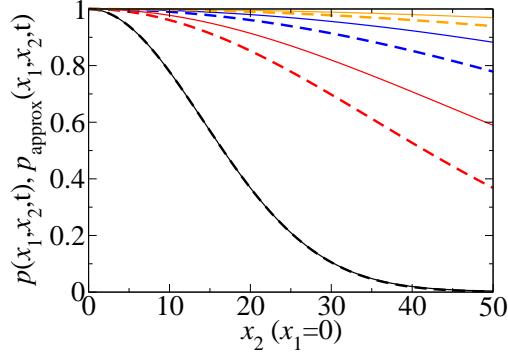


FIG. 2. This figure illustrates the role of Υ by comparing $p(x_1, x_2, t)$ and $p_{\text{appr}}(x_1, x_2, t)$. Solid curves correspond to $p(x_1, x_2, t)$, whereas dashed lines correspond to $p_{\text{appr}}(x_1, x_2, \Delta, t)$. We have taken, from top to bottom, $t = 10000, 2500, 625$, and 100 . For short times ($t = 100$), $p(x_1, x_2, t)$ and $p_{\text{appr}}(x_1, x_2, t)$ are seen to be almost identical.

where we have introduced the quantity

$$\Upsilon(x_2 - x_1, \Delta, t) \equiv \sum_{n=-\infty}^{\infty} \exp\left(\frac{-n^2 \Delta^2 + n(x_2 - x_1)\Delta}{2Dt}\right) \quad (51)$$

upon using the decomposition $R(x_2 - x_1, \Delta) = \Theta(x_2 - x_1)\Theta(\Delta - (x_2 - x_1))$ of the rectangular function as a product of two Heaviside functions. The prefactor $\Upsilon(x_2 - x_1, \Delta, t) \Theta(x_1 + \Delta - x_2)$ describes the effect of the finite reach of the motion due to the Δ -constraint. This prefactor can also be expressed as follows:

$$\Upsilon(x_2 - x_1, \Delta, t) = \frac{(2\pi Dt)^{1/2} e^{(x_2 - x_1)^2 / 8Dt}}{\Delta} \vartheta_3\left(-\frac{\pi(x_2 - x_1)}{2\Delta}, e^{-2\pi^2 Dt / \Delta^2}\right), \quad (52)$$

where $\vartheta_3(\cdot, \cdot)$ stands for an elliptic function. Note that the exact two-particle pdf $p(x_1, x_2, t)$ given by Eq. (50) can be rewritten in terms of the approximate pdf $p_{\text{appr}}(x_1, x_2, t)$ [which corresponds to $p_x(x_1, x_2, t; \Delta)$ as given by Eq. (1)] in this way:

$$p(x_1, x_2, t) = \Upsilon(x_2 - x_1, \Delta, t) p_{\text{appr}}(x_1, x_2, t). \quad (53)$$

Thus, the factor $\Upsilon(x_2 - x_1, \Delta, t)$ is a measure of quality of our proposal (1).

Figure 2 shows a comparison between the exact solution $p(x_1, x_2, \Delta, t)$ and $p_{\text{appr}}(x_1, x_2, \Delta, t)$ as a function of $x_2 - x_1$ for a fixed value $\Delta = 50$ and different times. Our approximation shows an extremely good agreement with the exact solution at short times; at longer times

it clearly underestimates the real pdf, but the agreement improves again at longer times and becomes acceptable provided that the value of $x_2 - x_1$ is not too large.

Numerically exact results for the reduced probabilities $p_1^{(1)}(x_1, t)$ and $p_2^{(1)}(x_2, t)$ can now be obtained by insertion of (50) into the definition of these quantities for the special case $N = 2$, namely,

$$p_1^{(1)}(x_1, t) = \int_{-\infty}^{\infty} dx_2 p(x_1, x_2, t), \quad (54)$$

$$p_2^{(1)}(x_1, t) = \int_{-\infty}^{\infty} dx_1 p(x_1, x_2, t). \quad (55)$$

Inserting Eq. (50) into the above expressions and performing the corresponding integration, one finally obtains (in full notation)

$$p_1^{(1)}(x_1, t, \Delta) = \left\{ \sum_{n=-\infty}^{\infty} e^{-n^2 \Delta^2 / (4Dt)} e^{-nx_1 \Delta / (2Dt)} \times \right. \\ \left. \times \left[\text{Erf} \left(\frac{x_1 + \Delta - n\Delta}{\sqrt{4Dt}} \right) - \text{Erf} \left(\frac{x_1 - n\Delta}{\sqrt{4Dt}} \right) \right] \right\} \frac{e^{-x_1^2 / 4Dt}}{\sqrt{4\pi Dt}} \quad (56)$$

for the left particle. The corresponding expression for the right particle is $p_1^{(2)}(x_2, t, \Delta) = -p_1^{(1)}(x_2, t, -\Delta)$. It is interesting to note that, leaving aside the normalization constant, our approximation (16) is obtained from the exact expression by retaining only the first term ($n = 0$) of the series. The terms with $n \neq 0$ are corrective decay modes whose contribution becomes most significant in the intermediate-time regime.

Finally, we note that it is straightforward to obtain an exact expression for $p(x_1, x_2, t)$ in the case of arbitrary non-zero initial particle separation (see Appendix B).

C. Exact moments

We now proceed to discuss the behavior of the first-order and second-order positional moments, as well as of particle correlations. Numerically exact results obtained by Laplace inversion are also available when both particles evolve on a lattice (see Appendix C).

1. Interparticle distance and first-order positional moment

An important parameter to measure the relaxation of our system towards the equilibrium steady state is the distance between particles $L = x_2 - x_1$. The n -th moment of this quantity

is defined via the following integral:

$$\langle L^n \rangle = \int_{-\infty}^{\infty} dx_1 \int_{-\infty}^{\infty} dx_2 (x_2 - x_1)^n p(x_1, x_2, t). \quad (57)$$

where $p(x_1, x_2, t)$ is given by Eq. (50). An easy way to simplify this integral consists in switching to center-of-mass (c.o.m.) and relative coordinates. To this end, we define $X \equiv (x_1 + x_2)/2$ and $L = x_2 - x_1$, which yields $x_1 = X - (L/2)$ and $x_2 = X + (L/2)$. The corresponding Jacobian is $J(X, L) \equiv \partial(x_1, x_2)/\partial(X, L) = 1$. Using this transformation in (57), we see that the integral decouples into two independent integrals, i.e.,

$$\langle L^n \rangle = \int_{-\infty}^{\infty} dX P(X, t) \int_0^{\Delta} dL L^n P(L, t). \quad (58)$$

Here,

$$P(X, t) \equiv \frac{e^{-X^2/(2Dt)}}{\sqrt{2\pi Dt}}, \quad -\infty < X < \infty \quad (59)$$

and

$$P(L, t) \equiv \frac{1}{\Delta} \vartheta_3\left(-\frac{\pi L}{2\Delta}, \zeta\right), \quad 0 \leq L \leq \Delta \quad (60)$$

are, respectively, the pdfs for the c.o.m. coordinate and for the interparticle distance (for compactness, in the latter we have introduced the definition $\zeta = \zeta(\delta) \equiv \exp[-\pi^2/(2\delta^2)]$). In (58), the integral over X obviously reduces to unity because of the normalization property of the pdf, and one is then left with

$$\langle L^n \rangle = \frac{1}{\Delta} \int_0^{\Delta} dL L^n \vartheta_3\left(-\frac{\pi L}{2\Delta}, \zeta\right). \quad (61)$$

We may now use the series representation

$$\vartheta_3(u, q) = 1 + 2 \sum_{m=1}^{\infty} q^{m^2} \cos(2mu) \quad (62)$$

of the elliptic function to find

$$\langle L^n \rangle = \frac{\Delta^n}{n+1} + \frac{2}{\Delta} \sum_{m=1}^{\infty} \zeta^{m^2} \int_0^{\Delta} dL L^n \cos\left(\frac{\pi m L}{\Delta}\right). \quad (63)$$

The integrals on the rhs are expressible in terms of hypergeometric functions. However, more transparent expressions are obtained for the first low-order moments. In particular, for the first moment $n = 1$, one finds

$$\langle L \rangle = 2\langle x_2 \rangle = \frac{\Delta}{2} - \frac{4\Delta}{\pi^2} \sum_{m=1}^{\infty} \frac{\zeta^{(2m-1)^2}}{(2m-1)^2}, \quad (64)$$

or, in terms of the approach to the mean particle separation $\langle L \rangle_{eq} = \Delta/2$ in the equilibrium state,

$$\rho \equiv \frac{\langle L \rangle}{\langle L \rangle_{eq}} - 1 = -\frac{8}{\pi^2} \sum_{m=1}^{\infty} \frac{\zeta^{(2m-1)^2}}{(2m-1)^2}. \quad (65)$$

Writing out the first two terms explicitly, one gets

$$\rho(\zeta) = -\frac{8}{\pi^2} \zeta - \frac{8}{9\pi^2} \zeta^9 + \mathcal{O}(\zeta^{25}). \quad (66)$$

As for the second-order moment $\langle L^2 \rangle$ of the separation distance, we now make use of the fact that

$$\int_0^\Delta dx x^2 \cos\left(\frac{\pi m x}{\Delta}\right) = \frac{2\Delta^3 (-1)^m}{\pi^2 m^2} \quad (67)$$

to find

$$\frac{\langle L^2 \rangle}{\Delta^2} = \frac{1}{3} + \frac{4}{\pi^2} \sum_{m=1}^{\infty} (-1)^m \frac{\zeta^{m^2}}{m^2}. \quad (68)$$

Note that we recover the correct value $\langle L^2 \rangle = 0$ as $\delta \rightarrow \infty$ ($t \rightarrow 0$).

Finally, let us express $\langle x_2 \rangle = \langle L \rangle/2$ in terms of time:

$$\frac{\langle x_2 \rangle}{\Delta} = -\frac{\langle x_1 \rangle}{\Delta} = \frac{1}{4} - \frac{2}{\pi^2} \sum_{m=1}^{\infty} \frac{e^{-2\pi^2(2m-1)^2 Dt/\Delta^2}}{(2m-1)^2}, \quad (69)$$

i.e., one has exponential relaxation to the limiting value in the long-time regime. Note that this result is at odds with the inverse power-law relaxation predicted by Eq. (23). This discrepancy clearly unveils the limitations of the factorization ansatz: although it is able to reproduce the correct limiting value of $\langle x_{1,2} \rangle$, it is too crude to predict the correct relaxation behavior.

In order to extract the short-time behavior from the rhs of Eq. (69), we take the Laplace transform, which yields

$$\frac{\langle \tilde{x}_2(s) \rangle}{\Delta} = \frac{1}{4s} - \frac{\Delta^2}{\pi^4 D} \sum_{m=1}^{\infty} \frac{1}{(2m-1)^2((2m-1)^2 + (\Delta^2 s)/(2\pi^2 D))}. \quad (70)$$

We can now take advantage of the result ([56], p. 689)

$$\sum_{m=1}^{\infty} \frac{1}{(2m-1)^2((2m-1)^2 + \mu^2)} = \frac{\pi^2}{8\mu^2} - \frac{\pi}{4\mu^3} \tanh \frac{\pi\mu}{2} \quad (71)$$

to obtain

$$\langle \tilde{x}_2(s) \rangle = \sqrt{\frac{D}{2s^3}} \tanh \sqrt{\frac{\Delta^2 s}{8D}} = \sqrt{\frac{D}{2s^3}} (1 - 2e^{-\sqrt{\frac{\Delta^2 s}{2D}}} + 2e^{-\sqrt{\frac{2\Delta^2 s}{D}}} + \mathcal{O}\left(e^{-\sqrt{\frac{9\Delta^2 s}{2D}}}\right)). \quad (72)$$

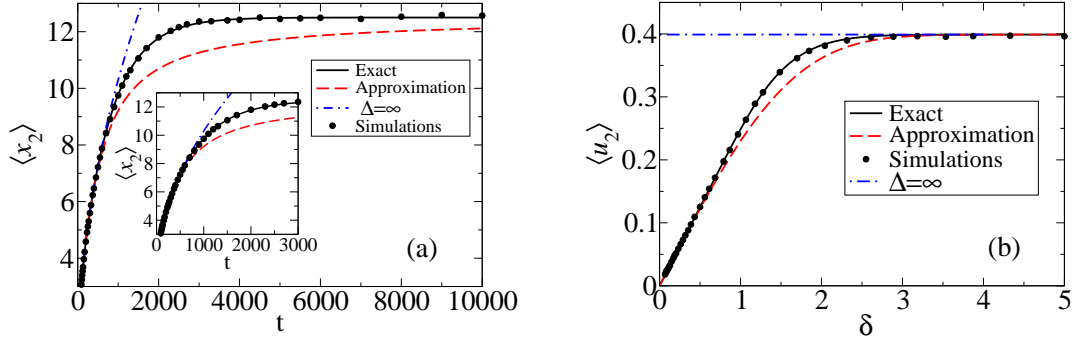


FIG. 3. Exact and approximate time dependence of $\langle x_2 \rangle$ (a) and δ -dependence of the scaled moment $\langle u_2 \rangle$ (b). For panel (a), we have used $\Delta = 50$ and $D = 1/6$. Circles correspond to simulation data that confirm the exact result. The inset on the left panel shows how the exact solution given by the solid line already starts to depart from the approximate one (dashed line) at relatively short times. The dot-dashed lines in both panels correspond to the exact solution for $\Delta = \infty$, i.e., $\langle x_2 \rangle = (2Dt/\pi)^{1/2}$ or, equivalently, $\langle u_2 \rangle = 1/(2\pi)^{1/2}$. Note that, for fixed values of Δ and D , increasing time t amounts to decreasing the value of δ , i.e., moving from the right to the left along the horizontal axis.

To retrieve the short-time behavior, we use the inverse transform

$$\mathcal{L}_s^{-1} \left\{ \frac{e^{-Cs^{1/2}}}{s^{3/2}} \right\} = \frac{2\sqrt{t}}{\pi} e^{-C^2/4t} + C \operatorname{Erf} \left(\frac{C}{2\sqrt{t}} \right) - C, \quad C > 0 \quad (73)$$

Finally, invoking the well-known asymptotic expansion of the error function for large arguments [cf. Eq. (32)], one eventually recovers Eq. (21), i.e.,

$$\langle x_2 \rangle = \frac{\langle L \rangle}{2} \approx \sqrt{\frac{2}{\pi} Dt} \left(1 - \frac{8Dt}{\Delta^2} e^{-\Delta^2/8Dt} \right). \quad (74)$$

Note the difference in the subleading term between the above expression and the one in Eq. (21). This signals once again the limitations of the factorization ansatz, which already fails to provide the correct prefactor of the subleading term.

Fig. 3(a) displays the time dependence of $\langle x_2 \rangle$. One clearly sees that the exact solution converges to the long-time limit $\Delta/4$ much faster than the approximate one. The exact result is confirmed by MC simulations. For completeness, we also show in Fig. 3(b) the universal curve of the scaled moment $\langle u_2 \rangle$ as a function of δ . In contrast with the curve for $\langle x_2(t) \rangle$, this latter curve does not depend on the specific values of Δ and D .

2. Second-order positional moment

The second-order moment follows immediately from the above decomposition in c.o.m. and relative coordinates. One has

$$\langle x_2^2 \rangle = \langle x_1^2 \rangle = \int_{-\infty}^{\infty} dx_1 \int_{-\infty}^{\infty} dx_2 x_2^2 p(x_1, x_2, t). \quad (75)$$

Taking into account that $p(x_1, x_2, t)dx_1dx_2 = p(X, L, t)dXdL = p(X, t)p(L, t)dXdL$, one has

$$\langle x_2^2 \rangle = \int_{-\infty}^{\infty} \int_0^{\Delta} dXdL \left(X + \frac{L}{2} \right)^2 p(X, t)p(L, t). \quad (76)$$

Thus,

$$\langle x_2^2 \rangle = \langle X^2 \rangle + \langle XL \rangle + \frac{\langle L^2 \rangle}{4} = \langle X^2 \rangle + \frac{\langle L^2 \rangle}{4}, \quad (77)$$

where we have used $\langle XL \rangle = \langle X \rangle \langle L \rangle$ and the fact that $\langle X \rangle = 0$ to derive the last equality. The c.o.m. performs a purely diffusive motion with diffusivity $D/2$; therefore, $\langle X^2 \rangle = Dt$, implying

$$\langle x_2^2 \rangle = Dt + \frac{\langle L^2 \rangle}{4}, \quad (78)$$

where $\langle L^2 \rangle$ is given by Eq. (68). As one can see, the (centered) MSD $\text{Var}(x_2)$ of the particle is directly related to the variance of the interparticle distance:

$$\text{Var}(x_2) = Dt + \frac{\text{Var}(L)}{4}. \quad (79)$$

In order to extract the short-time behavior, we need to assess how $\langle L^2 \rangle$ behaves in this limit. To this end, we note that, according to Eq. (68) the Laplace transform of $\langle L^2 \rangle$ is

$$\langle \widetilde{L^2}(s) \rangle = \frac{\Delta^2}{3s} + \frac{4\Delta^2}{\pi^2} \sum_{m=1}^{\infty} \frac{(-1)^m}{m^2 \left(\frac{2\pi^2 D m^2}{\Delta^2} + s \right)}. \quad (80)$$

We now use the result (see Ref. [56], p. 686)

$$\sum_{m=1}^{\infty} \frac{(-1)^m}{m^2 (m^2 + \mu^2)} = \frac{1}{2\mu^4} - \frac{\pi^2}{12\mu^2} - \frac{\pi \text{csch}(\pi\mu)}{2\mu^3}. \quad (81)$$

From the resulting large u behavior for $\langle \widetilde{L^2}(s) \rangle$, one then has

$$\langle \widetilde{L^2}(s) \rangle = \frac{4D}{s^2} - \sqrt{\frac{32\Delta^2 D}{s^3}} \left\{ e^{-\sqrt{\frac{\Delta^2 u}{2D}}} + \mathcal{O} \left(e^{-\sqrt{\frac{9\Delta^2 s}{2D}}} \right) \right\}. \quad (82)$$

The above behavior in Laplace space corresponds to the following short-time behavior:

$$\langle L^2 \rangle \approx 4Dt \left(1 - \sqrt{\frac{128Dt}{\pi\Delta^2}} e^{-\Delta^2/(8Dt)} \right). \quad (83)$$

Thus, at early times,

$$\text{Var}(x_2) \approx 2 \left(1 - \frac{1}{\pi} \right) Dt - \sqrt{\frac{128(Dt)^3}{\pi\Delta^2}} e^{-\Delta^2/(8Dt)}. \quad (84)$$

The first term corresponds to the result obtained by Aslangul [23] for $\Delta = \infty$. In the opposite limit of long times, it is easy to see that $\text{Var}(x_2) \rightarrow Dt = 2(D/2)t$, i.e., the diffusivity of each particle is decreased by a factor of two with respect to its value D for free particles.

Fig. 4(a) shows the time evolution of the variance $\text{Var}(x_2)$. The crossover from the early time value $2D(1-\pi^{-1})t$ to the late time value Dt is clearly seen. Note that these two regimes of normal diffusion at short and long-times have different diffusivities; they must therefore be connected to one another by a transient anomalous diffusion regime at intermediate times characterized by a nonlinear time dependence of the MSD. The approximate solution (dashed curve) deviates from the exact one at intermediate times. MC simulations (circles) are in good agreement with the theory. The difference between the approximate solution and the exact one becomes much more evident if one considers the scaled variance $\text{Var}(u) \equiv \text{Var}(x)/(4Dt)$ as a function of δ [see Fig. 4(b)].

3. Correlator

We are now in the position to obtain an exact expression for the two-particle correlation function $C(t) \equiv \langle x_1 x_2 \rangle - \langle x_1 \rangle \langle x_2 \rangle$. Making the replacement $x_1 = X - (L/2)$ and $x_2 = X + (L/2)$ in the corresponding expression, we find

$$C(t) = \langle X^2 \rangle - \frac{\text{Var}(L)}{4} = Dt - \frac{\text{Var}(L)}{4} = 2Dt - \text{Var}(x_2) \quad (85)$$

We thus see that the correlator, the MSD, and the variance of the relative coordinate are intimately connected to one another. In the short-time limit, one has

$$C(t) \approx \frac{2}{\pi} Dt + \sqrt{\frac{128(Dt)^3}{\pi\Delta^2}} e^{-\Delta^2/(8Dt)} \quad (86)$$

In contrast, one has $C(t) \approx Dt$ at long times.

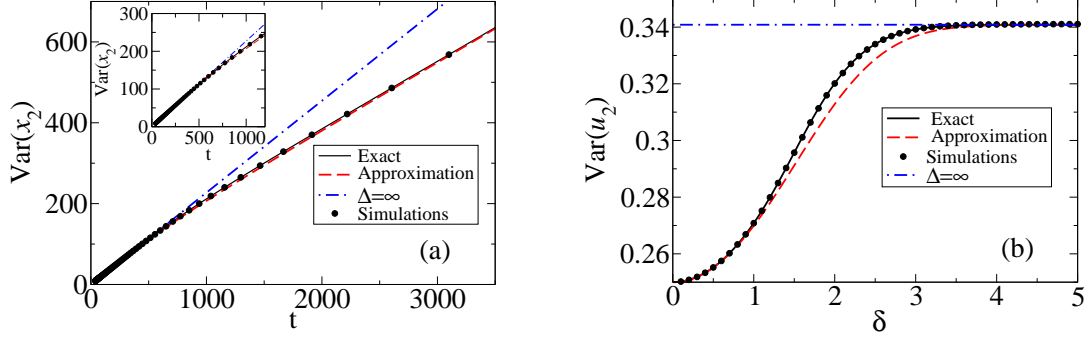


FIG. 4. Time evolution of the exact solution (solid line) and approximate solution (dashed line) for $\text{Var}(x_2)$ [panel (a)]. Displayed are also simulation results (circles). The inset displays the short time behavior. The corresponding solutions for $D_{\text{eff}}/D = \text{Var}(u_2)$ are also displayed as a function of δ [panel (b)]. The latter have been computed from data with $\Delta = 50$ and $D = 1/6$, but in the representation the analytical results collapse into the same curve regardless of the specific values of D and Δ . Dot-dashed lines in both panels correspond to the exact solution for $\Delta = \infty$, namely, $\text{Var}(x_2) = 2D(1 - \pi^{-1})t$ and $\text{Var}(u_2) = (1 - \pi^{-1})/2$.

Fig. 5(a) shows the crossover of the correlator from the early time value $(2/\pi)Dt$ to the late time value Dt . The deviations between the exact solution and the approximate one are once again clearly shown in the universal curve for the scaled correlator $c(\delta) \equiv \langle u_1 u_2 \rangle - \langle u_1 \rangle \langle u_2 \rangle = C(t)/(4Dt)$ with $t = t(\delta) = \Delta^2/(4D\delta)$ [see panel (b)].

V. $N = 3$ CASE

In the three-particle case, it does not seem possible to obtain an exact solution for the positional pdf and associated moments. We will therefore resort to the factorization ansatz introduced earlier to obtain approximate results, and we will assess the accuracy of this method by means of MC simulations. We focus again on the case of a fully packed initial condition (the three particles start from the origin).

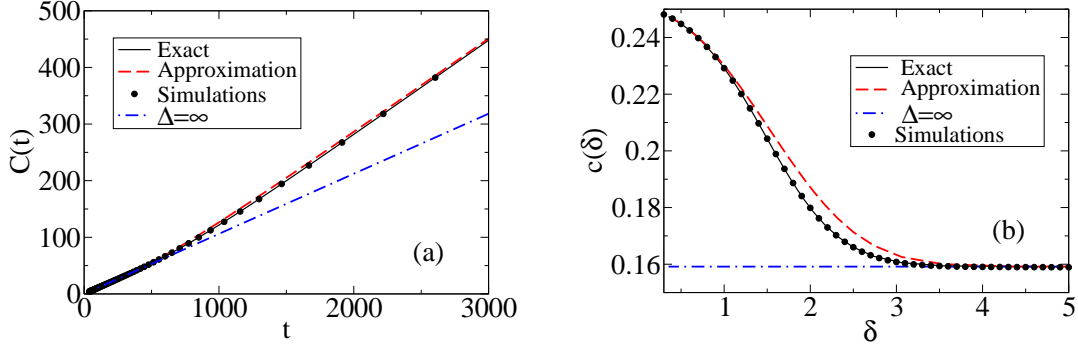


FIG. 5. Unscaled correlator $C(t)$ as a function of time (a), and scaled correlator $c(\delta)$ as a function of δ (b). Solid lines correspond to the exact solution, dashed lines to the approximate one. Dot-dashed lines correspond to the case $\Delta = \infty$. In this case $C(t) = (2/\pi)Dt$, and consequently $c(\delta) = 1/(2\pi)$.

A. General expressions for one-particle pdfs

The one-particle pdfs for the left- and rightmost particles (respectively labeled 1 and 3) are symmetric with respect to the origin and different from the pdf for the central particle (walker 2). In terms of scaled variables, the one-particle pdf for the leftmost particle takes the form

$$p_1^{(1)}(u_1, \delta) = A_1 e^{-u_1^2} \int_{u_1}^{u_1+\delta} du_2 e^{-u_2^2} \int_{u_2}^{u_2+\delta} du_3 e^{-u_3^2}, \quad (87)$$

where A_1 is a normalization constant (more generally, A_n will hereafter denote the normalization constant for the n -th one-particle pdf, see below). For $\delta \rightarrow \infty$ (short times or large Δ) one recovers Aslangul's result for $\Delta = \infty$ [23]:

$$p_1^{(1)}(u_1, \delta \rightarrow \infty) = \frac{\pi A_1}{8} e^{-u_1^2} [1 - \text{Erf}(u_1)]^2. \quad (88)$$

For completeness, even though no new physics is involved, we also give the pdf for the rightmost particle in the general case:

$$p_3^{(1)}(u_3, \delta) = A_3 e^{-u_3^2} \int_{u_3}^{u_3-\delta} du_2 e^{-u_2^2} \int_{u_2}^{u_2-\delta} du_1 e^{-u_1^2}. \quad (89)$$

As for the central particle, one has

$$p_2^{(1)}(u_2, \delta) = A_2 e^{-u_2^2} \int_{u_2}^{u_2-\delta} du_1 e^{-u_1^2} \int_{u_2}^{u_2+\delta} du_3 e^{-u_3^2}, \quad (90)$$

whence the $\Delta = \infty$ result already obtained by Aslangul follows [23]:

$$p_2^{(1)}(u_2, \delta \rightarrow \infty) = \frac{\pi A_2}{4} e^{-u_2^2} [1 + \text{Erf}(u_2)] [1 - \text{Erf}(u_2)]. \quad (91)$$

B. δ -expansion

By analogy with the procedure employed in the $N = 2$ case (see IIIB and IIIC), we now seek to obtain approximations for the reduced pdfs and the corresponding moments by means of a δ -expansion. To this end, we use the expansion $f(z) = f(u) + f'(u)(z - u) + \dots$ in integrals of the form $\int_u^{u \pm \delta} dz f(z)$, and then carry out the integration term by term. From Eq. (87), we find

$$p_1^{(1)}(u_1, \delta) = A_1 \sqrt{\frac{\pi}{3}} e^{-3u_1^2} \left[1 - 3u_1\delta - \frac{8}{9}(1 - 6u_1^2)\delta^2 + \dots \right] \quad (92)$$

for the leftmost particle. This yields the expansion

$$\langle u_1 \rangle = -\frac{\delta}{2} + \frac{\delta^3}{12} - \frac{\delta^5}{120} + \dots \quad (93)$$

for the first moment, implying $\langle u_1 \rangle = -\delta/2$ when $\delta \rightarrow 0$, e.g. in the long-time limit $t \rightarrow \infty$. Consequently, $\langle x_1 \rangle = -\Delta/2 = -\langle x_3 \rangle$ as $t \rightarrow \infty$.

Proceeding in a similar way for the second moment, we obtain the result

$$\langle u_1^2 \rangle = \frac{1}{6} + \frac{8\delta}{27} - \frac{85\delta^4}{972} + \dots \quad (94)$$

Note that $\langle u_1^2 \rangle = 1/6 = 1/(2N)$ in the limit of small δ . For the centered second-order moment, this implies $\text{Var}(x_1) \rightarrow 2Dt/3$ as $t \rightarrow \infty$, i.e., the effective diffusion coefficient of particle 1 tends to $D/3$ as $t \rightarrow \infty$ (which, by symmetry, is also the diffusion coefficient of particle 3).

The central particle 2 has, of course, a different dynamics, as it is confined by their two neighbors 1 and 3. The corresponding expansion yield

$$p_2^{(1)}(u_2, \delta) = A_2 \sqrt{\frac{\pi}{3}} e^{-3u_2^2} \left[1 - \frac{1}{18}(1 - 6u_2^2)\delta^2 + \frac{5 - 66u_2^2 + 72u_2^4}{1620}\delta^4 + \dots \right] \quad (95)$$

$$= A_2 \frac{\pi}{4} e^{-u_2^2} [\text{Erf}(u_2) - \text{Erf}(u_2 - \delta)] [\text{Erf}(u_2 + \delta) - \text{Erf}(u_2)] \quad (96)$$

for the pdf. The first-order moment vanishes trivially, $\langle u_2 \rangle = 0$, whereas the second-order moment can be expanded as follows:

$$\langle u_2^2 \rangle = \frac{1}{6} + \frac{\delta^2}{54} + \frac{\delta^4}{4860} + \dots \quad (97)$$

Thus, $\langle u_2^2 \rangle \rightarrow 1/6 \rightarrow 1/(2N)$ as $\delta \rightarrow 0$. This again implies $\text{Var}(x_2) \approx \text{Var}(x_1) \approx 2Dt/3$ at long times. Thus, the effective diffusion coefficient of the central particle is asymptotically the same as that of each neighbor $D_{2,\text{eff}} = D_{1,\text{eff}} = D_{3,\text{eff}} \rightarrow D/3$ as $t \rightarrow \infty$. In other words, at long times the three-particle system behaves as a single entity with the effective diffusion coefficient $D/N = D/3$. Moreover, as we will shortly see, this D/N -behavior at long times holds for arbitrary N .

C. Comparison with MC simulations

In order to assess the validity of the Gaussian (diffusive) approximation based on the factorization ansatz [cf. Eqs. (87) and (90)], we have performed numerical simulations for the particles' motion. In all cases, the waiting time distribution for the jumps of each walker is an exponential of mean $\tau = 1$, and the jump length pdf is a symmetric exponential with variance $2\ell^2 = 2$. The resulting diffusive constant is thus $D = \ell^2/\tau = 1$. For short times (up to $\sim 10\tau$) the Gaussian approximation is rather poor. However, the agreement improves at somewhat larger times, e.g. for times such that $\delta \approx 3$ (see Fig. 6). In Fig. 6 we compare simulation results for the reduced probabilities $p_m^{(1)}$'s (where $m = 1$ for the left particle and $m = 2$ for the central one) with the approximate reduced probabilities obtained by reexpressing Eqs. (87) and (90) in terms of the original (i.e., unscaled) space and time variables. Both for the left and the central particle, the agreement between the approximate theory and the numerical pdfs is quite acceptable, but the effect of the Δ constraint in this time regime is not very relevant yet (the approximate analytical solutions overlap with the curves for $\Delta = \infty$, which are also displayed in Fig. 6).

The agreement between the simulations, the approximate solution and the $\Delta = \infty$ curve progressively worsens at longer times, as shown for the left particle in Fig. 7 in the time regime where δ varies from 2 to $1/3$. In this figure, one also sees that the agreement between the simulations and the approximate solution first deteriorates with increasing time [see panels (b) and (c)], yielding an important discrepancy at times for which $\delta \approx 1$. However, at larger times the agreement improves again (see panel (c) for the case $\delta = 1/3$).

Interestingly, the Gaussian approximation seems to perform better for the central particle than for the edge particle. Fig. 8 shows a comparison of the pdfs obtained from numerical simulations with curves computed from Eq. (90) for the same times as in Fig. 7. The

discrepancy between the simulation data and the approximate curves remains small as δ decreases from the value of 2 for $t = 156$ to the value of $1/3$ at $t = 5625$.

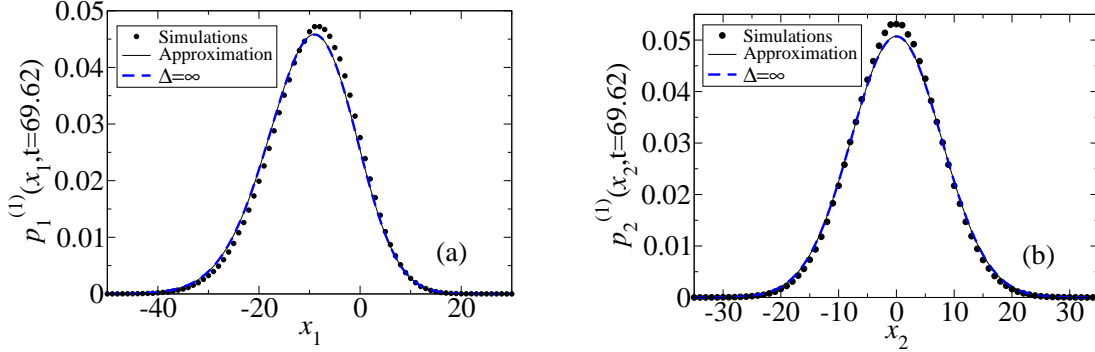


FIG. 6. Simulation results for $p_m^{(1)}(x, t, \Delta)$ with $D = 1$, $\Delta = 50$, $t = 69.62$ (i.e, a short time, corresponding to $\delta = 3$) and $N = 3$. Panel (a) corresponds to the left particle $m = 1$, whereas panel (b) corresponds to the central particle ($m = 2$). Solid lines correspond to the approximate solution, whereas dashed lines correspond to Aslangul's solution for $\Delta = \infty$.

VI. N-PARTICLE CASE

In this section, we present results for the general case of arbitrary N . To this end, we exploit the iterative relations between the integrals that appear in the general expressions for the one-particle pdfs.

A. Iterative formulas

The one-particle pdf for the m -th particle is

$$p_m^{(1)}(u_m; \delta) = A_m \int_{-\infty}^{\infty} du_1 \int_{-\infty}^{\infty} du_{m-1} \dots \int_{-\infty}^{\infty} du_{m+1} \int_{-\infty}^{\infty} du_N \prod_{i=1}^N e^{-u_i^2} \prod_{i=1}^{N-1} R(u_{i+1} - u_i, \delta) \quad (98)$$

i.e.,

$$p_m^{(1)}(u_m, \delta) = A_m e^{u_m^2} I_L(m-1, \delta; u_m) I_R(N-m, \delta; u_m), \quad (99)$$

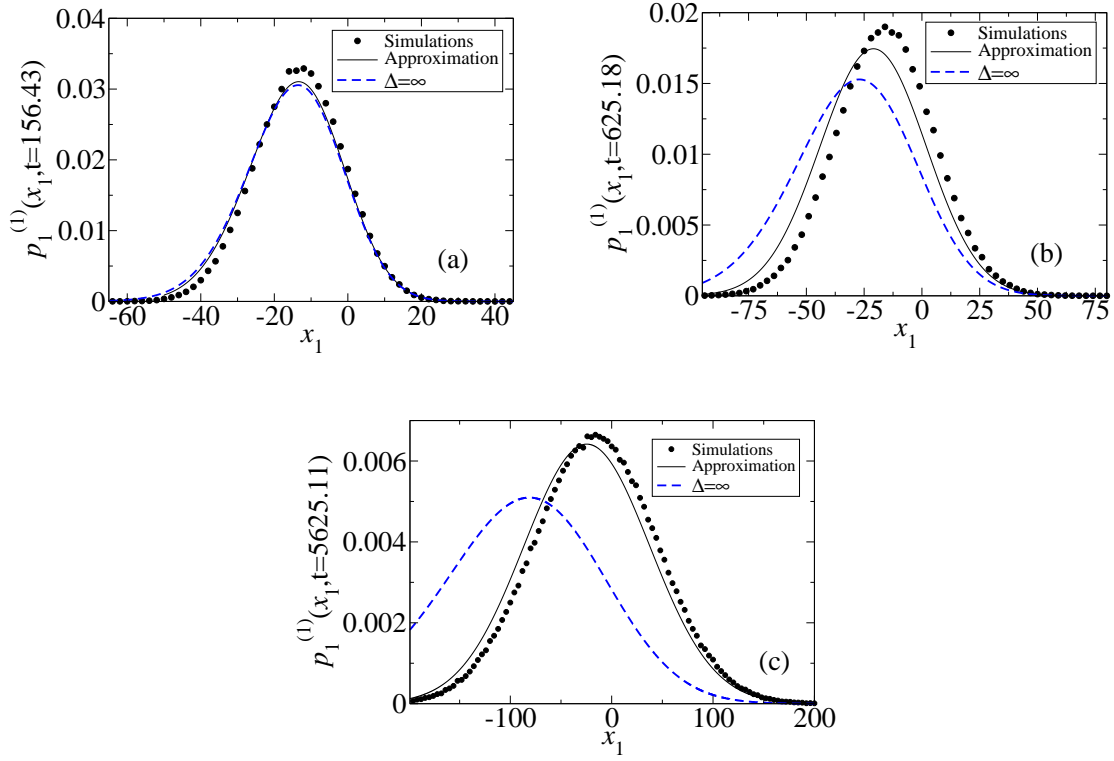


FIG. 7. Simulation vs. approximate analytical results for $p_1^{(1)}(x, t, \Delta)$ with $D = 1$ and $\Delta = 50$ for $t = 156.43$ ($\delta = 2$) (a), $t = 625.18$ ($\delta = 1$) (b) and $t = 5625.11$ ($\delta = 1/3$) (c) for three particles, $N = 3$. The dashed curves correspond to the analytical result for $\Delta = \infty$.

where

$$\begin{aligned}
 I_R(N - m, \delta; u_m) &= \int_{-\infty}^{\infty} du_{m+1} e^{-u_{m+1}^2} R(u_{m+1} - u_m, \delta) \dots \int_{-\infty}^{\infty} du_N e^{-u_N^2} R(u_N - u_{N-1}, \delta) \\
 &= \int_{u_m}^{u_m + \delta} du_{m+1} e^{-u_{m+1}^2} \dots \int_{u_{N-1}}^{u_{N-1} + \delta} du_N e^{-u_N^2}
 \end{aligned} \tag{100}$$

and

$$\begin{aligned}
 I_L(m - 1, \delta; u_m) &= \int_{-\infty}^{\infty} du_1 e^{-u_1^2} R(u_2 - u_1, \delta) \dots \int_{-\infty}^{\infty} du_{m-1} e^{-u_{m-1}^2} R(u_m - u_{m-1}, \delta) \\
 &= \int_{u_m - \delta}^{u_m} du_{m-1} e^{-u_{m-1}^2} \dots \int_{u_2 - \delta}^{u_2} du_1 e^{-u_1^2} \\
 &= (-1)^{m-1} \int_{u_m}^{u_m - \delta} du_{m-1} e^{-u_{m-1}^2} \dots \int_{u_2}^{u_2 - \delta} du_1 e^{-u_1^2}.
 \end{aligned} \tag{101}$$

For the particular case $\Delta = \infty$, Eq. (99) leads to Aslangul's result (cf. Eq. (3) in Ref. [23]).

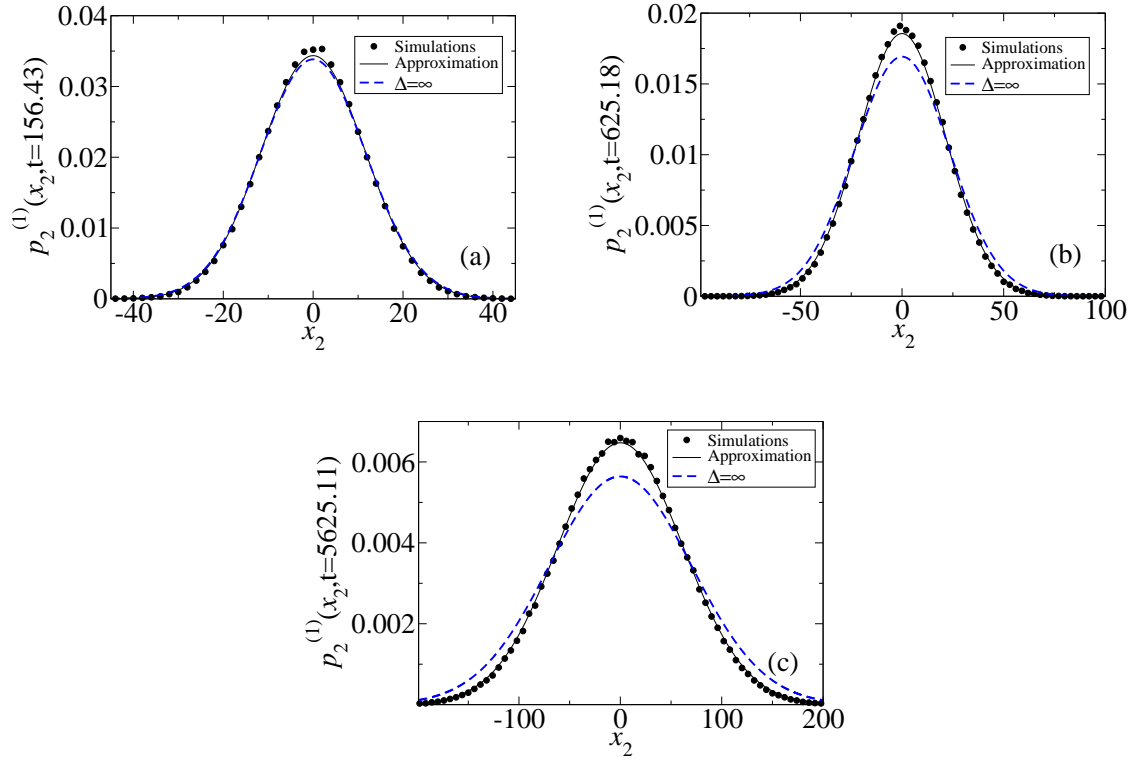


FIG. 8. Simulation vs approximate analytical results for $p_2^{(1)}(x, t, \Delta)$ with $D = 1$ and $\Delta = 50$ for $t = 156.43$ ($\delta = 2$) (a), $t = 625.18$ ($\delta = 1$) (b) and $t = 5625.11$ ($\delta = 1/3$) (c) for three particles, $N = 3$. The dashed curves correspond to the analytical result for $\Delta = \infty$.

To this end, one uses the explicit expressions

$$\int_u^\infty dz e^{-z^2} \text{Erfc}^n(z) = \frac{\sqrt{\pi}}{2(n+1)} \text{Erfc}^{n+1}(u), \quad n = 0, 1, \dots \quad (102)$$

and

$$\int_{-\infty}^u dz e^{-z^2} (1 + \text{Erf}(z))^n = \frac{\sqrt{\pi}}{2(n+1)} (1 + \text{Erf}(z))^{n+1}, \quad n = 0, 1, \dots \quad (103)$$

to respectively simplify the integrals $I_R(N - m, \infty; u_m)$ and $I_L(m - 1, \infty; u_m)$.

In order to deal with the case of finite δ , we observe that

$$I_L(n, \delta; u) = (-1)^n I_R(n, -\delta; u). \quad (104)$$

Therefore, Eq. (99) is equivalent to

$$p_m^{(1)}(u_m, \delta) = A_m e^{u_m^2} (-1)^{m-1} I_R(m - 1, -\delta; u_m) I_R(N - m, \delta; u_m). \quad (105)$$

On the other hand, one has

$$I_R(n, \delta; u) = \int_u^{u+\delta} du_1 e^{-u_1^2} I_R(n-1, \delta; u_1), \quad (106)$$

with $I_R(0, \delta; u) = 1$. We now express $I_R(n, \delta; u)$ in powers of δ by expanding $e^{-u_1^2} I_R(n-1, \delta; u_1)$ about u and carrying out the integration term by term. The result is

$$I_R(n, \delta; u) = \sum_{k=0}^{\infty} \frac{\delta^{k+1}}{(k+1)!} \frac{d^k}{du^k} \left\{ e^{-u^2} I_R(n-1, \delta; u) \right\}. \quad (107)$$

We thus arrive at an *iterative* formula that turns out to be very convenient for the evaluation of the series expansion of $I_R(n, \delta; u)$ in powers of δ . By means of Eq. (107), it is not difficult to compute the δ -expansions of the first two moments (for the central particle and the leftmost particle) for large values of N (e.g., up to $N = 200$). In this way we find

$$\langle u_1 \rangle = -\frac{N-1}{4} \delta - \frac{N(1-N^2)}{288} \delta^3 + \mathcal{O}(\delta^5), \quad (108)$$

$$\langle u_1^2 \rangle = \frac{1}{2N} + \frac{2+3N-14N^2+9N^3}{144N} \delta^2 + \mathcal{O}(\delta^4) \quad (109)$$

$$\langle u_{\text{central}}^2 \rangle \equiv \langle u_{\lfloor \frac{N}{2} \rfloor}^2 \rangle = \frac{1}{2N} + \frac{N^2-1}{144N} \delta^2 + \mathcal{O}(\delta^4). \quad (110)$$

In Eq. (110), $\lfloor \dots \rfloor$ denotes the floor function.

The constant term $(2N)^{-1}$ obtained in Eqs. (109) and (110) confirms the D/N asymptotic behavior already observed for $N = 2$ and $N = 3$, i.e., each particle moves with an effective diffusivity D/N . The $1/N$ dependence of $D_{\lfloor \frac{N}{2} \rfloor, \text{eff}}$ is in qualitative agreement with Aslangul's findings for the $\Delta = \infty$ case; however, in the case of the edge particles, the behavior is different, since Aslangul obtained a much slower decay of the effective diffusivity with N , $D_{1, \text{eff}} = D_{N, \text{eff}} \propto D/\ln(N)$ in the large N limit. As we see, the Δ constraint induces a much faster decrease of the diffusivity of the edge particles with increasing particle number, and it also homogenizes the behavior of the collection of particles. The common diffusivity D/N is also a well-known result of an ideal model of polymers (e.g., the Rouse model), where D is the diffusivity of a single (free) monomer.

We close the present subsection by noting that, in view of the above results based on (107), one might be led to think that it is possible to obtain general asymptotically exact expressions for the N -dependence of the moments. However, this hope is greatly reduced by the practical difficulties encountered during the evaluation procedure of the nested integrals.

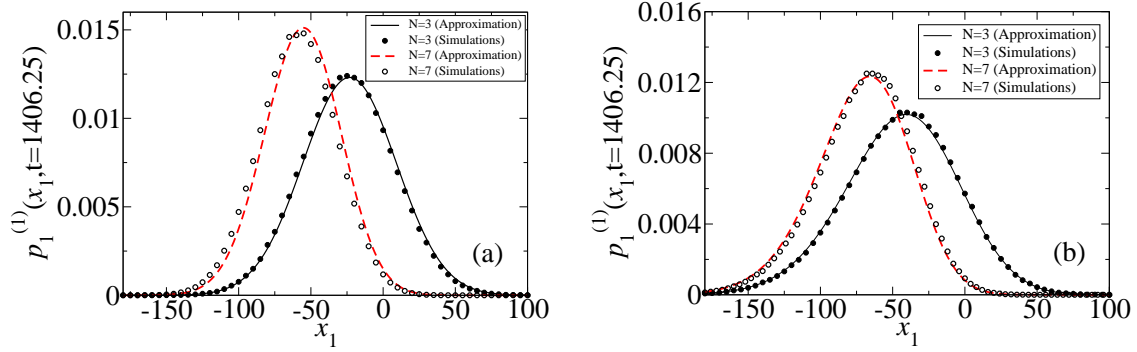


FIG. 9. Behavior of the leftmost particle. Open and filled circles correspond to simulation results, solid and dashed lines to the approximate analytical solutions. The values $D = 1$ and $\Delta = 200$ have been used.

B. Comparison between approximate theory and MC simulations

Figure 9 displays a comparison between the behavior of the leftmost particle for $N = 3$ and for $N = 7$. Both simulation results and approximate solutions based on the factorization ansatz are shown (see VI A). Panel (a) corresponds to $\Delta = 50$, whereas panel (b) corresponds to $\Delta = 7500$. The time has been set to $t = 1406.25$, and the diffusivity D to unity, respectively leading to $\delta = 2/3$ [panel (a)] and to $\delta = 100$ [panel (b)]. One can see that the approximation agrees very well with the simulations for $N = 3$, and the agreement is still good for $N = 7$. For a given value of Δ , one clearly sees that the leftmost particle is drifted further away from the origin with increasing N because of the increased push of a larger number of particles. For a given value of N , the peak of the pdf is also found to move to the left with increasing Δ , as a larger value of this quantity implies that the leftmost particle has a less severe restriction to move in the negative direction of the real axis (increasing Δ has, however, a stronger effect for $N = 3$ than for $N = 7$).

Similar plots for the pdf of the central particle $p(x_{\text{central}}, t) \equiv p_{[N/2]}^{(1)}(x_{[N/2]}, t)$ are shown in Fig. 10 (the parameters for panels (a) and (b) in this figure are the same as those used in Fig. 9 for the leftmost particle). As expected, the localization of the central particle becomes stronger with increasing N , as a larger number of particles enhances the confinement effects. For a given N , the pdf is higher and narrower (i.e., more localized) for a smaller value of Δ because of the stronger confinement induced by the mutual interactions.

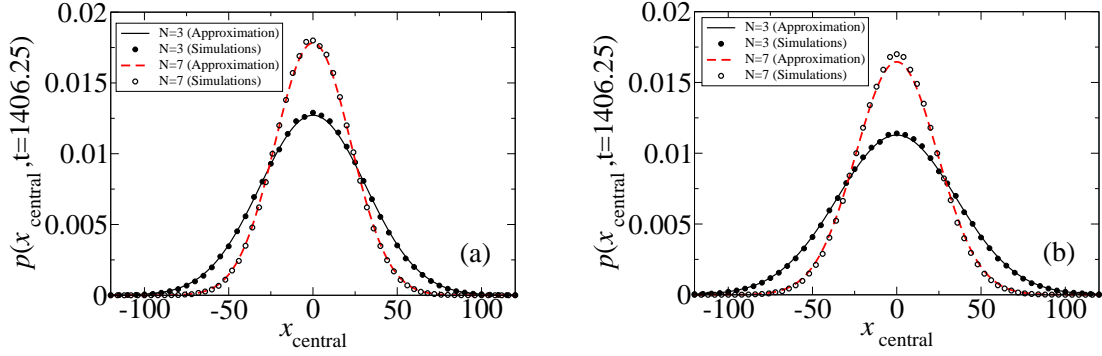


FIG. 10. Behavior of the central particle. Open and filled circles correspond to simulation results, solid and dashed lines to the approximate analytical solutions. Here, again, the values $D = 1$ and $\Delta = 200$ have been used.

C. Relaxation to the equilibrium state

1. Prediction based on factorization ansatz

For small $\delta = \Delta/\sqrt{4Dt}$ (e.g., in the long time limit), our factorization ansatz provides analytical expressions for $\langle u_1 \rangle$ and, by symmetry, also for $\langle u_N \rangle = -\langle u_1 \rangle$. Using Eq. (108), one finds

$$\frac{\langle x_1 \rangle}{\Delta} = -\frac{N-1}{4} + \frac{N(N^2-1)}{288} \delta^2 + \mathcal{O}(\delta^4). \quad (111)$$

In terms of the time t , we thus have

$$\frac{\langle x_1 \rangle}{\Delta} = -\frac{N-1}{4} + \frac{N(N^2-1)}{288} \frac{\Delta^2}{4Dt} + \mathcal{O}\left(\frac{\Delta^2}{4Dt}\right)^2. \quad (112)$$

The average length (end-to-end distance) of our system is $\langle L \rangle = \langle x_N - x_1 \rangle = 2|\langle x_1 \rangle| = -2\langle x_1 \rangle$. Eq. (112) then gives

$$\frac{\langle L \rangle}{\Delta} = \frac{N-1}{2} - \frac{N(N^2-1)}{144} \frac{\Delta^2}{4Dt} + \mathcal{O}\left(\frac{\Delta^2}{4Dt}\right)^2. \quad (113)$$

In terms of the average equilibrium system length, $\langle L \rangle_{\text{eq}} = (N-1)\Delta/2$ (see Sec. VII), this result can be rewritten as follows:

$$\frac{\langle L \rangle}{\langle L \rangle_{\text{eq}}} = 1 - \frac{N(N+1)}{72} \frac{\Delta^2}{4Dt} + \mathcal{O}\left(\frac{\Delta^2}{4Dt}\right)^2. \quad (114)$$

Thus, the Gaussian approximation predicts that the long-time approach to the equilibrium length is dictated by an inverse-power law:

$$\frac{\langle L \rangle - \langle L \rangle_{\text{eq}}}{\Delta} \propto \frac{\Delta^2}{4Dt}, \quad t \gg \Delta^2/D. \quad (115)$$

Note, however, that this prediction based on the factorization ansatz contradicts the exact result (69), which yields exponential relaxation in the long time limit for the specific case $N = 2$.

For large N , Eq. (114) becomes

$$\frac{\langle L \rangle}{\langle L \rangle_{\text{eq}}} = 1 - \frac{N^2}{72} \frac{\Delta^2}{4Dt} + \mathcal{O}\left(\frac{\Delta^2}{4Dt}\right)^2, \quad N \gg 1. \quad (116)$$

On the basis of the above results, one would expect that the time (relaxation time τ_r) required to reach a given fraction of the equilibrium length (99%, say) scales as $N^2\Delta^2/D$ for large N , that is, as $\tau_r \sim \langle L \rangle_{\text{eq}}^2/D$. In spite of the peculiar form of the particle-particle interactions in our system (string-bead chain), it is interesting to note that this result coincides with the one yielded by the Rouse model for an ideal polymer chain [51].

As for higher-order moments, we note that the computation of $\langle L^2 \rangle$ requires the evaluation of the corresponding correlator $\langle x_N x_1 \rangle$, since $\langle L^2 \rangle = \langle (x_N - x_1)^2 \rangle = \langle x_N^2 \rangle + \langle x_1^2 \rangle - 2\langle x_N x_1 \rangle = 2\langle x_1^2 \rangle - 2\langle x_N x_1 \rangle$. While $\langle x_1^2 \rangle$ can be evaluated approximately in the framework of the factorization ansatz, it does not seem possible to obtain explicit results for the integrals appearing in the definition of the correlator in the case of arbitrary $N > 2$ (in contrast, we recall that the case $N = 2$ is amenable to analytical treatment, see IV C 3).

2. Comparison with MC simulations

In order to assess the analytical predictions of VIC 1, we have performed numerical simulations for different values of N . As it turns out, the simulation results *contradict* the predictions of the Gaussian approximation and thus question its validity in the long-time regime. Rather than an inverse power law decay, one finds an *exponential* long-time ($\delta \rightarrow 0$) decay in the long limit $\delta \rightarrow 0$:

$$\log \left[\frac{|\langle L \rangle - \langle L \rangle_{\text{eq}}|}{\langle L \rangle_{\text{eq}}} \right] \sim -\frac{c(N)}{N^2\delta^2} \sim -c(N) \frac{t}{\tau_r} \quad (117)$$

This divergence in the limit of small δ explains the failure of an expansion of $\langle L \rangle$ in terms of this parameter. According to our numerical estimates (cf. Fig. 11), the function $c(N)$

depends only weakly on N and seems to converge to a common value $c(\infty)$ when N increases. The exponential relaxation observed at long times is strongly at odds with the much slower $1/t$ asymptotic decay predicted in VIC 1, but in line with the exact analytic result obtained for $N = 2$ and in the Rouse model. We thus see that the Gaussian approximation not only fails to predict the correct relaxation behavior for $N = 2$, but also for larger N . In any case, our string-bead model demonstrates that, while assuming an elastic interaction between the beads proves useful for a detailed analysis of relaxation modes, it is not essential for observing exponential relaxation. The abrupt interactions considered here are, in fact, quite different from those prescribed by harmonic potentials.

Finally, note that in Fig. 12 the relaxation time τ_r needed to practically reach the equilibrium state scales in such a way that $N\delta_{\text{eq}} \approx 2$, where $\delta_{\text{eq}} = \Delta/\sqrt{4D\tau_r}$; in other words, $\tau_r \approx \langle L \rangle_{\text{eq}}^2/(4D)$, in agreement with the Rouse model [51] (as pointed out in Sec. VIC 1).

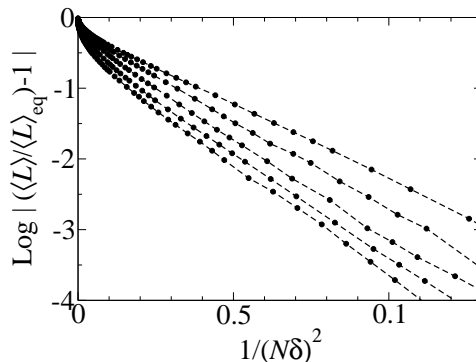


FIG. 11. Simulation results for the relaxation of the (properly scaled) average end-to-end distance $\langle L \rangle$ as a function of $1/(N\delta)^2$. The curves correspond, from top to bottom, to the values $N = 2, 3, 5, 11, 101$. For the first four curves we have taken $\Delta = 200$, whereas for $N = 101$ we have chosen $\Delta = 50$. In all cases, $D = 1$. The lines are an aid to the eye.

3. Role of the initial condition

In Fig. 13 we show simulation results describing the relaxation towards the equilibrium state for $N = 5$. Specifically, the horizontal axis represents the values of t in units of $\Delta^2/(2D)$, i.e., the dimensionless time $t_\Delta = (2D/\Delta^2)t$. The vertical axis represents different

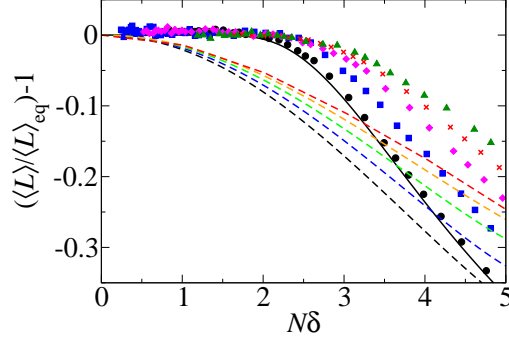


FIG. 12. Relaxation of $\langle L \rangle$ (properly scaled) as a function of $N\delta$. Notice that the equilibrium state is reached for $N\delta \approx 2$. Symbols correspond to data from numerical simulations (with $N = 101, 11, 5, 3, 2$ from top to bottom). The dashed lines depict the corresponding approximate solutions obtained from δ -expansions for the first order moment up to terms of order δ^{12} (again with $N = 101, 11, 5, 3, 2$ from top to bottom). The solid line corresponds to the solution provided by Eq. (65) for the $N = 2$ case.

functions of the mean end-to-end distance $\langle L(t) \rangle$ (i.e., the mean separation between the edge particles 1 and 5), so that all the curves take the value one for $t_\Delta = 0$ (see figure caption). We consider the case of a fully compressed initial condition treated so far (all particles start at $x = 0$), but also another initial arrangement where the particles are separated from each other by the maximum distance Δ (fully stretched initial condition). Fig. 13 shows that the relaxation for the fully stretched and the fully compressed initial conditions *is the same*. This behavior is also found in the Rouse model [51].

We also find that, in the early and intermediate time regimes, a fit to a simple monoexponential decay is not satisfactory. As is clearly seen in the semilog plot shown in Fig. 13, the numerical data deviate significantly from a straight line at short times, implying that the decay is more complicated than a simple exponential relaxation. This is in line with the analytical findings for $N = 2$ in this regime, which predict a multimodal decay [cf. Eq. (65)]. This is also similar to what happens in polymers, such as in the Rouse model, where the evolution of the polymer toward the equilibrium state is given in terms of a superposition of exponentially decaying modes, each of them with different characteristic decay time [51].

From Fig. 13 one clearly sees that the relaxation of the edge particles 1 and 5 (and of

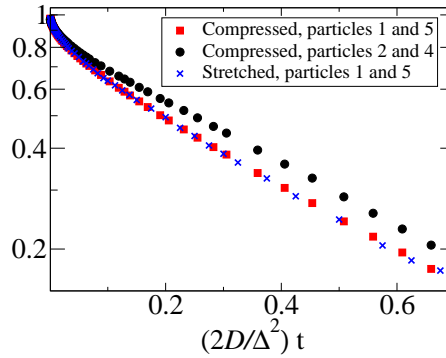


FIG. 13. Relaxation of $|\langle L(t) \rangle - \langle L \rangle_{\text{eq}}| / \langle L \rangle_{\text{eq}} = |1 - (\langle x_5 \rangle - \langle x_1 \rangle) / (2\Delta)|$ for a system with $N = 5$ (in this case $\langle L \rangle_{\text{eq}} = 2\Delta$) for stretched initial condition ($L(0) = 4\Delta = 2\langle L \rangle_{\text{eq}}$; crosses) and compressed initial condition ($L(0) = 0$; squares). Relaxation of the distance between the *neighbors* of the edge particles $[\Delta - (\langle x_4 \rangle - \langle x_2 \rangle)] / \Delta$ for the compressed initial condition (circles). For the simulations, the values $D = 1$ and $\Delta = 200$ have been used.

the depicted linear combinations thereof) is clearly different from that of particles 2 and 4. This is sensible because particles 2 and 4 have two nearest neighbors, whereas particles 1 and 5 only have a single neighbor to interact with during the relaxation process.

VII. CHARACTERIZATION OF THE EQUILIBRIUM STATE

So far, we have mainly discussed relaxation properties without giving many details about the final state beyond macroscopic properties such as the first moments of the end-to-end distance L (recall that $\langle L \rangle = -2\langle x_1 \rangle = 2\langle x_N \rangle$ for odd N) or the long-time asymptotic diffusion coefficient of the system as a whole. We have already noted in Sec. VIA that the diffusion coefficient of the tethered chain depends on N as in the Rouse model of polymers. We have also found in Sec. VIC 1 that the long-time relaxation of the tethered chain scales with the diffusivity D and with N (or equivalently with its length) as in the Rouse model.

In this section, we will further explore the possible similarities of the tethered chain with an ideal polymer. To this end, we will compute the number of states (microstates) compatible with a given size of the chain at equilibrium, whence we shall infer the exact distribution of this quantity, as well as the entropy and the Helmholtz free energy of our system. It turns

out that the tethered chain follows a linear relationship between an applied force and the change in the end-to-end distance (Hooke’s law), as it is the case in ideal polymer models such as the spring-bead chain (Rouse model), where the interaction between neighboring beads is mediated by harmonic springs.

The above finding is at first sight surprising given the striking differences between the tethered (string-bead) chain and the spring-bead model. First, note that the spring-bead model, in the absence of thermal noise, has a well-defined mechanical equilibrium length (the length equal to the sum of the distances between successive beads when the springs connecting them are neither stretched nor compressed). In the tethered chain, however, there is no mechanical equilibrium length. In fact, if the thermal noise were zero, one would find that the system length could take any value between zero and $N\Delta$, and the separation distances between nearest-neighbor beads would then take any value between 0 and Δ . In other words, in the tethered chain, the beads do not rattle (due to the thermal noise) about a mechanical equilibrium position (determined by elastic forces between beads). Thus, the energy of this “string-bead system” does not depend on the specific configuration. In this respect, this one-dimensional model resembles ideal three-dimensional models (such as the freely rotating chain model) of polymers. [50, 54].

A. Microstates and associated equilibrium probabilities

In this section, we count the number of states (microstates) of a tethered chain with a given N and Δ that are compatible with a chain length L at equilibrium [In this section, for brevity, we use the notation $\langle L \rangle$ instead of the mean (or ensemble average) $\langle L \rangle_{\text{eq}}$]. Each microstate is characterized by the set $\{r_1, \dots, r_{N-1}\}$ of $N - 1$ interparticle distances ($r_i = x_{i+1} - x_i$). The corresponding macroscopic variable is the length $L = \sum_{i=1}^{N-1} r_i$ of the chain. The set of relevant macrovariables then is $\{L, N, \Delta\}$.

For our reasoning below, we consider a microscopic lattice with unit mesh size $a = 1$. In addition, we assume that each lattice site can be occupied by a single particle at most, and that each particle symmetrically attempts to perform jumps to nearest-neighbor sites in continuous time subject to this restriction and to the Δ constraint. When implementing the latter constraint we will adopt the microscopic rule that the separation between any two neighboring particles cannot become equal to Δ , i.e., its maximum value is $\Delta - 1$. Similarly,

the minimum value of the separation between two neighboring particles is 1. Jump attempts implying same site occupation or violation of this constraint result in the resetting of the chosen particle to its starting position.

If one does not fix the value of L , the number of possible microstates (i.e., the number of different relative positions $\{r_1, \dots, r_{N-1}\}$ of the N particles in the lattice) is $\Omega \equiv (\Delta-1)^{N-1}$. Of course $\Omega = \sum_L \Omega(L, N, \Delta)$ where $\Omega(L, N, \Delta)$ denotes the number of microstates with a given value of L (and N and Δ).

The task of computing $\Omega(L, N, \Delta)$ can be tackled using standard combinatorial arguments. Note that $\Omega(L, N+1, \Delta+1)$ can be seen as the number of different ways, $\{r_1, \dots, r_N\}$, to obtain the sum $L = \sum_i^N r_i$ (with $N \leq L \leq N\Delta$) when rolling N dice if the outcome r_i of each die is restricted to the set of values $1, 2, \dots, \Delta$. The solution of this classic combinatorial problem is [57]:

$$\Omega(L, N+1, \Delta+1) = \sum_{k=0}^{\lfloor \frac{L-N}{\Delta} \rfloor} (-1)^k \binom{N}{k} \binom{L-k\Delta-1}{N-1}. \quad (118)$$

Because the probability of each microstate $\{r_1, \dots, r_N\}$ is the same, the probability of having a chain of length L is $p(L, N+1, \Delta+1) = \Omega(L, N, \Delta)/\Omega$, that is,

$$p(L, N+1, \Delta+1) = \Delta^{-N} \sum_{k=0}^{\lfloor \frac{L-N}{\Delta} \rfloor} (-1)^k \binom{N}{k} \binom{L-k\Delta-1}{N-1}. \quad (119)$$

For the chain with macrovariables $\{L, N+1, \Delta+1\}$ the mean value of L of the system length is $\langle L \rangle = N(\Delta+1)/2$ and its variance is $\sigma^2 = N(\Delta^2-1)/12$. Note that, because L comes from the sum of N independent variables, r_i , the mean and variance of L are the mean, $(\Delta+1)/2$, and variance, $(\Delta^2-1)/12$, of r_i multiplied by a factor N .

Equation (119) gives us the exact probability of finding a tethered chain of length L . However, it is not very useful when N is very large. Fortunately, in the large- N limit this probability can be very well approximated in the form of a Gaussian distribution centered on $\langle L \rangle$ and with variance σ^2 . For large N and Δ one can approximate the average and variance of the length by $N\Delta/2$ and $N\Delta^2/12$, respectively, and one gets

$$p(L, N, \Delta) \approx \frac{1}{\sqrt{\pi N \Delta^2 / 6}} \exp \left[-\frac{(L - N\Delta/2)^2}{N\Delta^2/6} \right]. \quad (120)$$

B. Statistical thermodynamics

We now assume that the diffusive (Brownian) motion of the particles (beads) of the tethered (or string-bead) chain is due to the thermal forces coming from the medium (bath) in which the chain is located. According to Einstein's fluctuation-dissipation relation, $D = k_B T / \xi$, where k_B is the Boltzmann constant, T is the temperature of the bath, and ξ is the friction coefficient.

The entropy of the tethered chain $S(L, N, \Delta) = k_B \ln \Omega(L, N, \Delta)$ is obtained from the relation $\Omega(L, N, \Delta) = p(L, N, \Delta) \Delta^{N-1}$ and from Eq. (120):

$$S(L, N, \Delta) = -k_B \frac{6(L - \langle L \rangle)^2}{N\Delta^2} - k_B \ln \left(\frac{\pi N \Delta^2}{6} \right) + k_B (N - 1) \ln \Delta. \quad (121)$$

The Helmholtz free energy of the chain is $F = U - TS$ where the U energy of the chain. Note that, as in models of ideal polymers [54], U does not depend on L because the particles (beads) in the allowed configurations have no interaction energy. This means that, according to Eq. (121), the free energy of the tethered chain increases quadratically with L . This implies, as in the ideal chain polymer models, that the elasticity of the tethered chain satisfies Hooke's law: the force f required to stretch the chain a length $x = L - \langle L \rangle$ from the averaged (equilibrium) value $\langle L \rangle$ is proportional to x ,

$$f = k_B T \frac{\partial F}{\partial L} = \frac{6k_B T}{N\Delta^2} (L - \langle L \rangle). \quad (122)$$

The associated (entropic) spring constant is $C_L = 6k_B T / (N\Delta^2)$. Taking into account that $\ell = \langle r_i \rangle = \Delta/2$ is the mean particle separation at equilibrium, the elastic constant can be rewritten as $C_L = 3k_B T / (2N\ell^2)$, that is just the expression of the spring constant for ideal polymers [54]. Note that the force f and the associated spring constant C_L are completely of entropic origin, since there is no elastic interaction and hence no springs modeling mechanical forces between the beads in our string-bead chain.

VIII. SUMMARY AND OUTLOOK

Let us briefly recap the main results of this paper. Inspired by Aslangul's work [23], we have considered a one-dimensional system of N Brownian walkers undergoing SFD, but subject to the additional constraint that the separation distance of any two walkers cannot exceed the threshold value Δ (we have coined the term "tethered walkers" to reflect

this constraint). The dynamics displays remarkable differences with respect to the $\Delta = \infty$ case treated by Aslangul; for finite Δ , a factorization ansatz describes reasonably well the behavior of reduced pdfs over a wide range of parameters, but fails to capture other features such as long-time relaxation properties. As we have seen, an exact solution can only be found for $N = 2$ case (an exact solution for the on-lattice case is also available in Laplace space). The first positional moment relaxes exponentially to the equilibrium state at long times, as opposed to the inverse power law behavior predicted by our ansatz. The MSD of either particle behaves linearly at short and long times, but with different (yet Δ -independent) diffusion coefficients (at intermediate times, transient anomalous diffusion is observed). Another effect of introducing a maximum interparticle distance Δ is an expected enhancement of particle-particle correlations, which has been precisely quantified from the exact solution.

For arbitrary $N > 2$, an iterative procedure has been developed to compute the one-particle pdf of any particle and the positional moments (in the latter case, as a power series in terms of $\delta = \Delta/\sqrt{4Dt}$). The resulting single-particle pdfs accurately capture the corresponding simulation results, both qualitatively and, in many cases (especially for short and long times), quantitatively.

In the long time regime, every particle in the system moves with an effective diffusivity $\propto 1/N$, as opposed to the large- N behavior $\propto 1/\ln(N)$ observed in the $\Delta = \infty$ case for the edge particles [23]. According to our analytical findings for $N = 2$, the positional first-order moment for each particle decays exponentially at long times; this result is also obtained in numerical simulations for $N > 2$, the relaxation time being $\tau_r = N^2\Delta^2/4D = \langle L \rangle_{\text{eq}}^2/D$. Finally, we have discussed the statistical properties of the equilibrium state, i.e., the state reached when $t \rightarrow \infty$ where the average system length does not depend on time. Using combinatorial arguments, we have evaluated the number of microstates compatible with a given system length, the probability of this length, the associated mean and variance, and the entropy of the chain and the force needed to change it by a given amount. As in the Rouse spring-bead model, it turns out that this (entropic) force is Hookean despite the non-analyticity of the interaction potential imposed by the Δ -constraint.

The present problem can be extended in many directions. One could e.g. investigate in a more comprehensive manner the role of different initial conditions. One could also consider the effect of an external force [31, 58–60], which would amount to replacing the

unbiased Gaussian solution for each individual particle in the factorization ansatz by the corresponding biased propagator. Finally, our approach can also be adapted to the situation where the maximum separation Δ_L between a given particle and its left neighbor is different from the maximum allowed distance Δ_R to the right neighbor. Moreover, one could even consider the case where either Δ_L or Δ_R becomes infinite, while the other unilateral reach remains finite.

IX. ACKNOWLEDGEMENTS

S. B. Y. and E. A. acknowledge financial support from Grant No. PID2020-112936GB-I00 funded by MCIN/AEI/10.13039/501100011033. A. B. thanks the Department of Physics of the University of Extremadura for its hospitality.

APPENDIX A: ARBITRARY ODD-ORDER MOMENTS FOR $N = 2$

In this appendix, we will obtain analytic expressions for the odd-order moments of the approximate single-particle pdf proposed (factorization ansatz) in Sec. III A for the case $N = 2$. To obtain the n -th order moment when $N = 2$, one must evaluate the following expression:

$$\langle u_2^n \rangle = \frac{1}{\sqrt{\pi} \operatorname{Erf}(\delta/\sqrt{2})} \left[\int_{-\infty}^{\infty} du_2 u_2^n \operatorname{Erf}(u_2) e^{-u_2^2} - \int_{-\infty}^{\infty} du_2 u_2^n \operatorname{Erf}(u_2 - \delta) e^{-u_2^2} \right]. \quad (123)$$

The analytic form of the first integral on the rhs of (123) is known. One has

$$\int_{-\infty}^{\infty} du_2 u_2^n \operatorname{Erf}(u_2) e^{-u_2^2} = \frac{2}{\sqrt{\pi}} {}_2F_1(1/2, n/2 + 1, 3/2, -1) \Gamma(n/2 + 1). \quad (124)$$

On the other hand, the second integral on the rhs of Eq. (123) can be expressed as a sum of Laplace transforms $\tilde{g}(s)$ of the function $g(z) = z^m \operatorname{Erf}(a\sqrt{z} + b)$ (where a and b are real constants and m is a positive integer) by performing the change of variable $z = u_2^2$ and subsequently setting the Laplace variable s equal to one. Given that [61]

$$\tilde{g}(s) = (-1)^m \frac{d^m}{ds^m} \left[\frac{1}{s} \operatorname{Erf}(b) + \frac{a}{s\sqrt{s+a^2}} e^{-b^2 s/(s+a^2)} \operatorname{Erfc} \left(\frac{ab}{\sqrt{s+a^2}} \right) \right], \quad (125)$$

we find, upon performing the pertinent simplifications,

$$\langle u_2^n \rangle = -\langle u_1^n \rangle = \frac{1}{\sqrt{\pi} \operatorname{Erf}(\delta/\sqrt{2})} \left[\frac{2}{\sqrt{\pi}} {}_2F_1(1/2, n/2 + 1, 3/2, -1) \Gamma(n/2 + 1) - (-1)^{(n-1)/2} \frac{d^{(n-1)/2}}{ds^{(n-1)/2}} \frac{1}{s\sqrt{1+s}} e^{-\delta^2 s/(1+s)} \Big|_{s=1} \right], \quad n \text{ odd.} \quad (126)$$

APPENDIX B: $N = 2$ CASE WITH A FINITE INITIAL PARTICLE SEPARATION

In what follows, our aim will be to compute the two-particle distribution $p(x_1, x_2, t)$ for the case where the initial interparticle distance d is strictly positive, thereby generalizing the $d = 0$ case described by Eq. (50) (without loss of generality, we will take $x_1(0) = 0$ and $x_2(0) = d$). In the $\Delta = \infty$ case, the solution for the corresponding problem with a reflecting horizontal boundary is given by:

$$p_\infty^{\text{hor}}(x_1, x_2, t) = \frac{e^{-(x_1 - \frac{d}{\sqrt{2}})^2/4Dt}}{4\pi Dt} \left(e^{-(x_2 - \frac{d}{\sqrt{2}})^2/4Dt} + e^{-(x_2 + \frac{d}{\sqrt{2}})^2/4Dt} \right) \Theta(x_2). \quad (127)$$

This solution satisfies the initial condition $p(x_1, x_2, 0) = \delta(x_1 - d/\sqrt{2}) \delta(x_2 - d/\sqrt{2})$ as well as the zero normal flux condition $\partial_{x_2} p(x_1, x_2, t)|_{x_2=0}$. The tilted solution

$$p_\infty(x_1, x_2, t) = \frac{e^{-(x_1+x_2-d)^2/8Dt}}{4\pi Dt} \left(e^{-(x_2-x_1-d)^2/8Dt} + e^{-(x_2-x_1+d)^2/8Dt} \right) \Theta(x_2 - x_1) \quad (128)$$

satisfies the imposed initial condition $p_\infty(x_1, x_2, 0) = \delta(x_1) \delta(x_2 - d)$, as well as the reflecting boundary condition $\mathbf{n}_\perp \cdot \nabla p_\infty(x_1, x_2, t)|_{x_2=x_1} = 0$. In the case of a finite reach Δ , the solution is more involved, but can again be obtained by a procedure similar to that for the case $x_1(0) = x_2(0) = 0$. To this end, one must consider the solution of the two-dimensional diffusion problem for two reflecting horizontal boundaries at $x_2 = 0$ and $x_2 = \Delta/\sqrt{2}$ and the particle starting at $(x_1(0), x_2(0)) = (d/\sqrt{2}, d/\sqrt{2})$. This particular initial condition is still covered by the general solution given in Ref. [55] (cf. Eq. (19) on p. 374), which reads

$$p^{\text{hor}}(x_1, x_2, t) = \sum_{n=-\infty}^{\infty} \left(e^{-(\sqrt{2}n\Delta + x_2 - \frac{d}{\sqrt{2}})^2/4Dt} + e^{-(\sqrt{2}n\Delta + x_2 + \frac{d}{\sqrt{2}})^2/4Dt} \right) \frac{e^{-(x_1 - \frac{d}{\sqrt{2}})^2/4Dt}}{4\pi Dt} R(x_2, \frac{\Delta}{\sqrt{2}}). \quad (129)$$

The solution for the initial condition $(0, d)$ is then found by tilting the above expression in the anticlockwise sense, which gives

$$p(x_1, x_2, t) = \sum_{n=-\infty}^{\infty} \left(e^{-(2n\Delta+x_2-x_1-d)^2/8Dt} + e^{-(2n\Delta+x_2-x_1+d)^2/8Dt} \right) \times \\ \times \frac{e^{-(x_1+x_2-d)^2/8Dt}}{4\pi Dt} R(x_2 - x_1, \Delta). \quad (130)$$

The above expression can be rewritten in terms of elliptic functions as follows:

$$p(x_1, x_2, t) = \frac{e^{-(x_2+x_1-d)^2/8Dt}}{\Delta(8\pi Dt)^{1/2}} \left[\vartheta_3 \left(\frac{\pi(x_2 - x_1 - d)}{2\Delta}, e^{-2\pi^2 Dt/\Delta^2} \right) + \right. \\ \left. + \vartheta_3 \left(\frac{\pi(x_2 - x_1 + d)}{2\Delta}, e^{-2\pi^2 Dt/\Delta^2} \right) \right] R(x_2 - x_1, \Delta). \quad (131)$$

APPENDIX C: ON-LATTICE SOLUTION FOR $N = 2$

It is interesting to characterize the differences between the dynamics of the continuum two-walker system and its corresponding lattice counterpart. An on-lattice solution for the $\Delta = \infty$ case was given by Aslangul [24]. He showed that lattice effects may persist up to unexpectedly long times. For finite Δ , we expect that the associated cage effect acts as an additional perturbation that makes for the particles even more difficult to reach a regime in which their motion is well described by continuum diffusion.

In order to study how lattice effects impact the behavior of positional moments, we consider that both particles start from contiguous sites on an infinite one-dimensional lattice with mesh size a . Let us label the lattice sites with consecutive integers. One of the particles starts at the origin (site 0), and the other one starts at the right neighbor site (site 1), say. Each particle performs a nearest-neighbor random walk in continuous time with symmetric hopping rate $2W$ (the one-sided jump rate is thus W , and consequently the single-particle diffusion coefficient becomes $D = Wa^2$). Following Aslangul [24], we neglect events where both particles jump during the same interval dt ; the dynamics is thus asynchronous. The single file constraint is implemented by precluding double site occupation; specifically, when a particle attempts to hop on a site that is already occupied by the other one, the jump is precluded and the particle remains at the same position. On the other hand, we implement the Δ -constraint on the discrete support as follows. The interparticle distance before an attempted particle jump is $(n_2 - n_1)a$, where n_1 and n_2 respectively denote the lattice sites

at which walker 1 and walker 2 are. If the interparticle separation becomes larger or equal than Δ as a result of an attempted jump by either particle, then no hopping takes place (this is consistent with the interaction rule used in Sect. VII A).

As in the continuum case (see IV C), it is possible to decompose the joint motion of the pair of particles in c.o.m. and relative coordinates. The evolution of the relative coordinate L may be viewed as that of a random walker of diffusivity $2D = 2Wa^2$ performing a nearest-neighbor walk on a one-dimensional lattice of spacing a and two reflecting end sites 0 and $N_\Delta = \Delta/a$ (we assume that Δ is a multiple of the lattice spacing a). Let us denote by $P_j^L(t)$ the probability that such a walker is found at site j (with $0 < j < N$) at time t and by $\tilde{P}_j^L(s)$ its Laplace transform with respect to time. Then, one has the result [62]:

$$\tilde{P}_j^L(s) = \frac{\cosh[\beta(N_\Delta - j - \frac{1}{2})] \cosh(\frac{\beta}{2})}{2W \sinh(\beta) \sinh[\beta(N_\Delta - 1)]}, \quad (132)$$

where $\beta = \cosh^{-1}(1 + (4W)^{-1}s)$. From Eq. (132), the calculation of Laplace-transformed moments of arbitrary order for the interparticle separation is immediate. One has

$$\langle \tilde{L}^n(s) \rangle = a^n \sum_{j=1}^{N_\Delta-1} j^n \tilde{P}_j^L(s). \quad (133)$$

It does not seem possible to derive an exact analytical expression for these moments in the time domain, since neither the above sum nor the individual $\tilde{P}_j^L(s)$'s are easy to invert. For $n = 1$ the sum evaluates to the following expression:

$$\langle \tilde{L}(s) \rangle = \frac{\sqrt{2a^2W} \operatorname{sech}[\frac{N_\Delta-1}{2} \cosh^{-1}(1 + \frac{s}{4W})] \sinh[\frac{N_\Delta}{2} \cosh^{-1}(1 + \frac{s}{4W})]}{s^{3/2}}. \quad (134)$$

Likewise, for $n = 2$, a lengthy expression in terms of hyperbolic trigonometric functions is obtained. In general, one must resort to numerical inversion to obtain results in the time domain. However, asymptotic analytic results for the short-time behavior can be obtained via Tauberian theorems. For $n = 1$, one has e.g. the general result

$$\langle L(t) \rangle = 2\langle x_2 \rangle - a = a \left\{ 1 + 2Wt - \sum_{j=2}^{\infty} (-1)^j c_j (Wt)^j \right\}, \quad (135)$$

where the coefficients $c_j > 0$ do not depend on N_Δ up to $j \geq N_\Delta - 1$. Thus, a finite value of Δ impacts the term of order $(Wt)^{N_\Delta-1}$ and the higher-order ones, while the lower-order terms remain the same as for $\Delta = \infty$ (of course, the effect of a finite Δ is to decrease $\langle L(t) \rangle$ at a given time t). Note that the first drift term [second term in the rhs of Eq. (135)] is

linear in time, in agreement with Aslangul's result for $\Delta = \infty$ (cf. Ref. [24]). As expected, at early times the particle drift is slowed down with respect to the off-lattice case, which is proportional to \sqrt{t} to dominant order, and therefore faster than the linear time dependence obtained for on-lattice diffusion.

Let us now examine the behavior of the c.o.m. pdf. In this case, one may regard its motion as that of a random walker with the same jump rate $2W$ as the one for the interparticle distance, but effectively moving on an infinite one-dimensional lattice with spacing $a/2$ and starting at site 1. This walker's diffusivity is $2W(a/2)^2 = D/2$. The expression of the Laplace transformed probability $\tilde{P}_m^X(s)$ for the walker to be at site m is known in this case. One has [62]

$$\tilde{P}_m^X(s) = \frac{e^{-\beta|m-1|}}{4W \sinh \beta}. \quad (136)$$

In general, the evaluation of the associated positional moments of lattice walks is usually easier if one first carries out the corresponding sums in Laplace space, and then inverts the resulting expressions either exactly or in asymptotic regimes amenable to analysis via Tauberian theorems. However, the inverse-Laplace transform of $\tilde{P}_m^X(s)$ is well-known in the present case of a simple nearest-neighbor walk:

$$P_m^X(t) = e^{-4Wt} I_{|m-1|}(4Wt), \quad (137)$$

where $I_n(\cdot)$ denotes the n -th order modified Bessel function of the first kind. The P_m^X 's are indeed normalized, since $\sum_{m=-\infty}^{\infty} I_{|m-1|}(x) = \sum_{m=-\infty}^{\infty} I_{|m|}(x) = \exp(x)$. Now, the moments of the c.o.m. pdf can be computed from their definition either in Laplace space

$$\langle \tilde{X}^n(s) \rangle = \left(\frac{a}{2}\right)^n \sum_{j=-\infty}^{\infty} j^n \tilde{P}_j^X(s), \quad (138)$$

or directly in the time domain:

$$\langle X^n(t) \rangle = \left(\frac{a}{2}\right)^n \sum_{j=-\infty}^{\infty} j^n P_j^X(t). \quad (139)$$

The formulas given in subsection IV C continue to hold in the discrete case, except for the fact that one must now take into account that the first moment of the c.o.m. no longer

vanishes, $\langle X \rangle = a/2$. Thus, one has

$$\langle x_2 \rangle = \langle X \rangle + \frac{\langle L \rangle}{2} = \frac{a}{2} + \frac{\langle L \rangle}{2}, \quad (140)$$

$$\langle x_2^2 \rangle = \langle X^2 \rangle + \langle X \rangle \langle L \rangle + \frac{\langle L^2 \rangle}{4} = \langle X^2 \rangle + \frac{a}{2} \langle L \rangle + \frac{\langle L^2 \rangle}{4}, \quad (141)$$

$$\text{Var}(x_2) = \text{Var}(X) + \frac{\langle L^2 \rangle - \langle L \rangle^2}{4} = \langle X^2 \rangle - \frac{a^2}{4} + \frac{\langle L^2 \rangle - \langle L \rangle^2}{4}, \quad (142)$$

$$C(t) = \langle X^2 \rangle - \frac{\langle L^2 \rangle - \langle L \rangle^2}{4}. \quad (143)$$

The second moment

$$\langle X^2 \rangle = \frac{a^2}{4} \sum_{j=-\infty}^{\infty} j^2 P_j^X(t) \quad (144)$$

of the c.o.m. coordinate can be explicitly computed in the time domain. Using the identity

$$\sum_{m=-\infty}^{\infty} m^2 I_{|m-1|}(x) = e^x (x+1), \quad (145)$$

one easily finds $\langle X^2 \rangle = \frac{a^2}{4} + W a^2 t$, that is

$$\langle X^2 \rangle - \langle X \rangle^2 = W a^2 t \quad (146)$$

Finally, in order to compare with the continuum case, one must set $W = D/a^2$ in all of the above formulas (this expression leads to the c.o.m. diffusivity $D/2$, as it should). To perform the comparison in terms of scaled variables, one sets (as before) $\langle u_2^n \rangle = \langle x_2^n \rangle / (4Dt)^{n/2}$.

A comparison between the continuum solution and the on-lattice solution is shown in Fig. 14 at the level of the scaled first-order moment $\langle u_2(\delta) \rangle$. In the case of the lattice solution, one of course no longer has $\langle u_2 \rangle = -\langle u_1 \rangle$, but rather $\langle u_2 \rangle = -\langle u_1 \rangle + (\delta/\Delta)a$, and one must therefore consider these two solutions separately. However, both are seen to converge to the off-lattice solution when one takes the diffusive limit by simultaneously letting the mesh size a (in this case identical with the initial particle separation) go to zero and the unilateral hopping rate W increase so as to keep the value of the diffusivity $D = a^2 W$ constant (in the case of Fig. 14, we have taken $D = 1$). Recall that a fixed Δ implies decreasing values of δ with increasing time (large values of δ therefore correspond to early times). The differences between the on- and the off-lattice solution are most pronounced for large δ , corresponding to the early time regime. The results are confirmed by MC simulations (see Fig. 14).

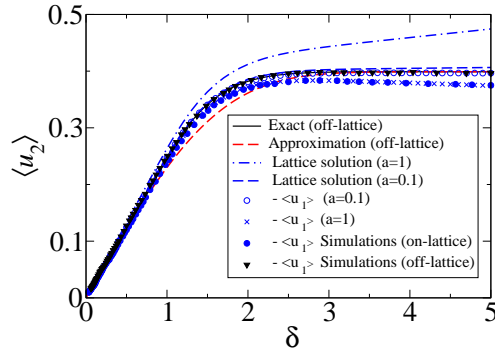


FIG. 14. Lattice solution for the scaled first-order moment $\langle u_2 \rangle$ of the right particle obtained from Eq. (140) and the numerical inversion of Eq. (134). We have used $\Delta = 50$. A comparison with the off-lattice solution is also included.

-
- [1] A. Ryabov, *Stochastic Dynamics and Energetics of Biomolecules* (Springer, Switzerland, 2016).
 - [2] O. Bénichou, P. Illien, G. Oshanin, A. Sarracino, and R. Voituriez, Tracer diffusion in crowded narrow channels, *J. Phys.: Condens. Matter* **30**, 443001 (2018).
 - [3] V. Gupta, S. S. Nivarthi, A. V. McCormick, and H. T. Davis, Evidence for single file diffusion of ethane in the molecular sieve $AlPO_4 - 5$, *Chem. Phys. Lett.* **247**, 596 (1995).
 - [4] T. Meersmann, J. W. Logan, R. Simonutti, S. Caldarelli, A. Comotti, P. Sozzani, L. G. Kaiser, and A. Pines, Exploring single-file diffusion in one-dimensional nanochannels by laser-polarized Xe-129 NMR spectroscopy, *J. Phys. Chem. A* **104**, 11665 (2000).
 - [5] D. W. Jepsen, Dynamics of a Simple Many-Body System of Hard Rods, *J. Math. Phys.* **6**, 405 (1965).
 - [6] D. G. Levitt, One-dimensional Time-Dependent Distributions, *J. Stat. Phys.* **7**, 329 (1973).
 - [7] D. Chowdhury, L. Santen, and A. Schadschneider, Statistical physics of vehicular traffic and some related systems, *Phys. Rep.* **329**, 199 (2000).
 - [8] A. Graneli, C. Yeykal, R. B. Robertson, and E. C. Greene, Long-distance lateral diffusion of human Rad51 on double-stranded DNA, *Proc. Natl. Acad. Sci. U.S.A.* **103**, 1221 (2006).
 - [9] G.-W. Li, O. G. Berg, and J. Elf, Effects of macromolecular crowding and DNA looping on

- gene regulation kinetics, Nat. Phys. **5**, 294 (2009).
- [10] A. John, A. Schadschneider, D. Chowdhury, and K. Nishinari, Trafficlike collective movement of ants on trails: absence of a jammed phase. Phys. Rev. Lett. **102**, 108001 (2009).
 - [11] P. C. Bressloff and J. M. Newby, Stochastic models of intracellular transport, Rev. Mod. Phys. **85**, 135 (2013).
 - [12] M. Muthukumar, *Polymer Translocation* (Boca Raton, Florida, CRC Press).
 - [13] T. T. Perkins, D. E. Smith, and S. Chu, Direct observation of tube-like motion of a single polymer chain, Science **264**, 819 (1994).
 - [14] K. Hahn, J. Kärger, and V. Kukla, Single-file diffusion observation, Phys.Rev. Lett. **76**, 2762 (1995).
 - [15] V. Kukla, J. Kornatowski, D. Demuth, I. Girnus, H. Pfeifer, L. V. C. Rees, S. Schunk, K. K. Unger, and J. Kärger, NMR studies of single-file diffusion in unidimensional channel zeolites, Science **272**, 702 (1996).
 - [16] D. Keffer, The temperature dependence of single-file separation mechanisms in onedimensional nanoporous materials, Chem. Eng. J. **74**, 33 (1999).
 - [17] J. Kärger, D. M. Ruthven, and D. N. Theodorou, *Diffusion in Nanoporous Materials (Vol. 1)*, (Wiley, Weinheim, 2012).
 - [18] C.-Y. Cheng and C. R. Bowers, Observation of Single-File diffusion in dipeptide nanotubes by continuous-flow hyperpolarized xenon-129 NMR spectroscopy, ChemPhysChem **8**, 2077 (2007).
 - [19] Q.-H. Wei, C. Bechinger, and P. Leiderer, Single-file diffusion of colloids in one-dimensional channels Science **287**, 625 (2000).
 - [20] R. N. Zia and J. F. Brady, Single-particle motion in colloids: force-induced diffusion, J. Fluid Mech. **658**, 188 (2010).
 - [21] M. Kollmann, Single-file Diffusion of Atomic and Colloidal Systems, Phys. Rev. Lett. **90**, 180602 (2003).
 - [22] C. Rödenbeck, J. Kärger, and C. Hahn, Calculating exact propagators in syngle file systems via the reflection principle, Phys. Rev. E **57**, 4382 (1998).
 - [23] C. Aslangul, Classical diffusion of N interacting particles in one dimension: General results and asymptotic laws, Europhys. Lett. **44**, 284 (1998).
 - [24] C. Aslangul, Diffusion of two repulsive particles in a one-dimensional lattice, J. Phys. A Math.

- Gen. **32**, 3993 (1999).
- [25] L. Lizana and T. Ambjörnsson, Single file diffusion in a box, Phys. Rev. Lett. **100**, 200601 (2008).
 - [26] L. Lizana and T. Ambjörnsson, Diffusion of finite-sized hard-core interacting particles in a one-dimensional box: Tagged particle dynamics, Phys. Rev. E **80**, 051103 (2009).
 - [27] P. Illien, O. Bénichou, C. Mejía-Monasterio, G. Oshanin, and R. Voituriez, Active Transport in Dense Diffusive Single-File Systems, Phys. Rev. Lett. **111**, 038102 (2013).
 - [28] A. Poncet, A. Grabsch, P. Illien, and O. Bénichou, Generalized Correlation Profiles in Single-File Systems, Phys. Rev. Lett. **127**, 220601 (2021).
 - [29] P. L. Krapivsky, K. Mallick, and T. Sadhu, Large Deviations in Single-File Diffusion, Phys. Rev. Lett. **113**, 078101 (2014).
 - [30] P. L. Krapivsky, K. Mallick, and T. Sadhu, Tagged Particle in Single-File Diffusion, J. Stat. Phys. **160**, 885 (2015).
 - [31] A. Lapolla and A. Godec, Unfolding tagged particle histories in single-file diffusion: exact single- and two-tag local times beyond large deviation theory, New J. Phys. **20**, 113021 (2018).
 - [32] E. Mallmin, J. du Buisson, and H. Touchette, Large deviations of currents in diffusions with reflective boundaries, J. Phys. A: Math. Theor. **54**, 295001 (2021).
 - [33] A. Grabsch, A. Poncet, P. Rizkallah, P. Illien, and O. Bénichou, Exact closure and solution for spatial correlations in single-file diffusion, Sci. Adv. **8**, eabm5043 (2022).
 - [34] A. Grabsch and O. Bénichou, Tracer Diffusion beyond Gaussian Behavior: Explicit Results for General Single-File Systems, Phys. Rev. Lett. **132**, 217101 (2024).
 - [35] L. P. Sanders and T. Ambjörnsson, First passage times for a tracer particle in single file diffusion and fractional Brownian motion, J. Chem. Phys. **136**, 175103 (2012).
 - [36] A. Lapolla, The First Exit Time Statistics and the Entropic Forces in Single File Diffusion, arXiv:2205.02339v1.
 - [37] T. E. Harris, Diffusion with “collisions” between particles, J. Appl. Prob. **2**, 323 (1965).
 - [38] L. Lizana, T. Ambjörnsson, A. Taloni, E. Barkai, and M. A. Lomholt, Foundation of fractional Langevin equation: Harmonization of a many-body problem, Phys. Rev. E **81**, 051118 (2010).
 - [39] R. Metzler and J. Klafter, The random walk’s guide to anomalous diffusion: a fractional dynamics approach, Phys Rep. **339**, 1 (2000).
 - [40] R. Metzler and J. Klafter, The restaurant at the end of the random walk: recent developments

- in the description of anomalous transport by fractional dynamics, *J. Phys. A Math. Gen.* **37**, R161 (2004).
- [41] R. Metzler, J.-H. Jeon, A. G. Cherstvy, and E. Barkai, Anomalous diffusion models and their properties: non-stationarity, non-ergodicity, and ageing at the centenary of single particle tracking, *Phys. Chem. Chem. Phys.* **16**, 24218 (2014).
 - [42] R. Metzler, L. Sanders, M. A. Lomholt, L. Lizana, K. Fogelmark, and T. Ambjörnsson, Ageing single file motion, *Eur. Phys. J. Spec. Top.* **223**, 3287 (2014).
 - [43] D. G. Levitt, Interpretation of Biological Ion channel flux data: Reaction-Rate versus Continuum Theory, *Ann. Rev. Biophys. Biophys. Chem.* **15**, 29 (1986).
 - [44] R. W. Bauer and W. Nadler, Molecular transport through channels and pores: Effects of in-channel interactions and blocking, *Proc. Natl. Acad. Sci. U.S.A.* **103**, 11447 (2006).
 - [45] E. Abad, J. Reingruber, and M. S. P. Sansom, On a novel rate theory for transport in narrow ion channels and its application to the study of flux optimization via geometric effects, *J. Chem. Phys.* **130**, 085101 (2009).
 - [46] A. V. Skorokhod, Stochastic equations for diffusion processes in a bounded region, *Theory Probab. Appl.* **6**, 264 (1961).
 - [47] D. S. Grebenkov, NMR survey of reflected Brownian motion, *Rev. Mod. Phys.* **79**, 1077 (2007).
 - [48] D. S. Grebenkov, Residence times and other functionals of reflected Brownian motion, *Phys. Rev. E* **76**, 041139 (2007).
 - [49] D. S. Grebenkov, Probability distribution of the boundary local time of reflected Brownian motion in Euclidean domains, *Phys. Rev. E* **100**, 062110 (2019).
 - [50] M. Doi and S. F. Edwards, *The Theory of Polymer Dynamics* (Oxford University Press, New York, 1986).
 - [51] A. J. Grosberg and A. R. Khokhlov, *Statistical physics of macromolecules* (AIP Press, Woodbury, New York, 1994)
 - [52] J.-B. Delfau, C. Coste, and M. Saint Jean, Single-file diffusion of particles in a box: Transient behaviors, *Phys. Rev. E* **85**, 061111 (2012).
 - [53] M. Abramowitz and I. Stegun, *Handbook of Mathematical Functions* (Dover, 1972), p. 297.
 - [54] M. Rubinstein and R. H. Colby, *Polymer Physics* (Oxford University Press, New York, 2003).
 - [55] H. S. Carslaw and J. C. Jaeger, *Conduction of Heat in Solids*, 2nd. ed. (Clarendon Press, Oxford, 1959).

- [56] A. P. Prudnikov, Yu. A. Brychkov, and O. I. Marichev, *Integrals and series, Vol. 1: Elementary functions* (Gordon and Breach, Amsterdam, 1998), p. 689.
- [57] J.V. Uspensky, *Introduction to Mathematical Probability* (McGraw-Hill, New York, 1937), pp. 23-24 (Problem 13).
- [58] E. Barkai and R. Silbey, Theory of Single File Diffusion in a Force Field, *Phys. Rev. Lett.* **102**, 050602 (2009).
- [59] E. Barkai and R. Silbey, Diffusion of tagged particle in an exclusion process, *Phys. Rev. E* **81**, 041129 (2010).
- [60] A. Lapolla and A. Godec, Manifestations of Projection-Induced Memory: General Theory and the Tilted Single File, *Front. Phys.* **7**, 182 (2019).
- [61] A. P. Prudnikov, Yu. A. Brychkov, and O. I. Marichev, *Integrals and series, Vol. 4: Direct Laplace transforms* (Gordon and Breach, Amsterdam, 1992), p. 173.
- [62] R. M. Mazo, On the Green's Function for a One-Dimensional Random Walk, *Cell Biophys.* **11**, 19 (1987).